Contract No:

This document was prepared in conjunction with work accomplished under Contract No. DE-AC09-08SR22470 with the U.S. Department of Energy (DOE) Office of Environmental Management (EM).

Disclaimer:

Large Plate Experiment of Chloride-induced Stress Corrosion Cracking in Spent Nuclear Fuel Storage Canisters

Spent Fuel and Waste Disposition

Prepared for
U.S. Department of Energy
Spent Fuel and Waste Science and Technology

Poh-Sang Lam
Andrew J. Duncan
Robert L. Sindelar
Savannah River National Laboratory

Charles R. Bryan
Sandia National Laboratories

September 5, 2020

Milestone No. M3SF-20SR010207022
SRNL-STI-2020-00315

Prepared by
Savannah River National Laboratory
Savannah River Nuclear Solutions
Aiken, South Carolina 29808

Savannah River National Laboratory is a multiprogram laboratory managed and operated by Savannah River Nuclear Solutions, LLC, for the U.S. Department of Energy under contract DE-AC09-09SR22505.

EXECUTIVE SUMMARY

This report provides a description of the testing (in progress at the Savannah River National Laboratory) to evaluate the corrosion behavior of a large section of welded plate material harvested from the Sandia National Laboratories' full-size mockup of a spent nuclear fuel (SNF) dry storage canister. The details of the establishment of this plate test, the interim corrosion results (from visual examination), and the general plan for examination of the plate in CY21 to evaluate crack growth behavior (if any) are provided. This work is intended to inform aging management programs for SNF canisters under conditions of extended dry storage.

A "large plate" (approximately 51×46 cm with thickness 16 mm and weight about 30 kg) and containing a circumferential weldment from the mockup is the test specimen. The knowledge of the salt, temperature, humidity conditions for chloride-induced stress corrosion cracking (CISCC) including the threshold stress intensity factor, K_{ISCC}, were used to setup the large plate test in which a set of part-through-wall and through-wall electrical discharge machined (EDM) defects were positioned in the weld residual stress field of the welded plate material from the mockup canister. A marine salt solution was applied to this plate specimen with an air-brush spray, then dried, and then exposed to a sustained 71-73% RH condition at an ambient room temperature of 22 °C. The salt loading and environmental condition is expected to be aggressive to cause CISCC.

The visual examination of the surface of the plate show clear evidence of corrosion product staining (brown rust appearance) but with no apparent cracking emanating from the machined notches after approximately 16 months exposure to date (test start May 8, 2019).

The plate test will continue in FY21. Following a total exposure of 2-years, non-destructive examination (NDE) and destructive examination (DE) characterization will be undertaken to identify and characterize cracking that may emanate from the machined defects (e.g. at the edges of the notches beneath the surface of the plate). The results from DE characterization of cracking will be used to verify NDE characterization results, and to develop effective through-wall crack growth rates from cracks that would likely be branched.

Related work to investigate CISCC initiation using "big plate" tests conducted at Sandia National Laboratories is briefly summarized. The Sandia plates were under more aggressive exposure conditions ($MgCl_2$ salt load at 80 °C with 35% RH), but the plates do not contain machined starter cracks. After 12 months exposure, no CISCC was observed even though the plates were fully covered by corrosion products.

The corrosion staining results have been compared to a standard for visual appearance that index corrosion severity. A Japanese Industrial Standard, JIS G 0595, was cited in ASME code case N-860 ("Inspection Requirements and Evaluation Standards for Spent Nuclear Fuel Storage and Transportation Containment Systems") as a visual indicator to trigger additional flaw characterization. Although the staining results from the plate testing at both SRNL and SNL are

considered “major corrosion,” no correlation of CISCC incidence to the JIS index can be made based on the present results of no-cracking reported in the testing.

This report fulfills the M3 milestone M3SF-20SR010207022, “Summary Report of the Canister Plate Corrosion Crack Growth Testing” under Work Package Number SF-20SR01020702.

ACKNOWLEDGMENTS

The authors gratefully acknowledge the support of Ned Larson, U.S. Department of Energy, Office of Nuclear Energy, Office of Spent Fuel and Waste Disposition, Office of Spent Fuel & Waste Science and Technology, for his office's sponsorship of this work, including the collaboration with Korea University under the I-NERI program. The authors thank the corrosion expert staff from Sandia National Laboratories (Rebecca Schaller and Andrew Knight) and the Pacific Northwest National Laboratory (Mychailo Toloczko) for helpful discussions throughout the course of this work.

The authors are grateful for the corrosion consultation and advice from our colleagues at the Savannah River National Laboratory, Bruce Wiersma, John Mickalonis, and for laboratory testing support from Lisa Ward.

The authors give an extra special acknowledgment to our partners at Korea University (Seoul, Republic of Korea), Professor Yun-Jae Kim and his students, for their companion work and supporting fracture mechanics analyses.

This page is intentionally left blank

CONTENTS

LIST OF FIGURES

LIST OF TABLES

ACRONYMS

AMP	Aging Management Program
API	American Petroleum Institute
ASME	American Society of Mechanical Engineers
BLCT	Bolt-load Compact Tension (specimen)
BM	Base metal
BPVC	Boiler and Pressure Vessel Code
CISCC	Chloride-Induced Stress Corrosion Cracking
CGR	Crack Growth Rate
COD	Crack opening displacement
CRIEPI	Central Research Institute of Electric Power Industry (Japan)
CT	Compact Tension Specimen
DAS	Data acquisition system
DOE	US Department of Energy
EDM	Electrical Discharge Machining
EIS	Electrochemical Impedance Spectroscopy
EPRI	Electric Power Research Institute
GW	Guided Wave
HAZ	Heat Affected Zone
ISFSI	Independent Spent Fuel Storage Installation
I-NERI	International Nuclear Energy Research Initiative
JIS	Japanese Industrial Standard
KU	Korea University
LWR	Light Water Reactor
NDE	Nondestructive Examination
NE	Nuclear Energy
NRC	Nuclear Regulatory Commission
PAUT	Phased Array Ultrasonic Test
PL	Pulsed Laser
PNNL	Pacific Northwest National Laboratory
PS	Proof Stress (Stress at 0.2% strain)
PT	Liquid Dye Penetrant Testing

PZT	Piezoelectric Transducer
RH	Relative Humidity
RN	Rating Number
SAW	Submerged arc welding
SCC	Stress Corrosion Cracking
SIF	Stress Intensity Factor
SLDV	Scanning Laser Doppler Vibrometer
SNF	Spent Nuclear Fuel
SNL	Sandia National Laboratories
SRNL	Savannah River National Laboratory
UT	Ultrasonic Test
VT	Visual Inspection
WRS	Welding Residual Stress
XRD	X-ray Diffraction

1. INTRODUCTION

Nearly 3000 spent nuclear fuel (SNF) dry storage canisters are currently in the Independent Spent Fuel Storage Installations (ISFSIs) in the United States. Because the canisters are not required to be stress relieved after welding and fabrication, stress corrosion cracking (SCC) has been identified as a potential concern due to the possibility of through-wall penetration that could breach the confinement boundary provided by the canisters. For canisters at ISFSIs near coastal regions, chloride-bearing salts may deposit on the external surface of the canister. Typically, the heat from radioactive decay at the time the dry storage canisters were loaded with SNF provides a canister with sufficient thermal mass to maintain the surface temperatures above the temperatures that allow deliquescence of atmospheric salts to occur[1], thereby limiting the occurrence of the surface brine, which is essential for the onset of chloride-induced stress corrosion cracking (CISCC). As canisters cool, surface temperatures will drop below this threshold in the long-term storage. If the local relative humidity at the canister surface is high enough, salt deposits may deliquesce and form aggressive brine. With the welding residual stress (WRS) as the driving force, CISCC may take place in the weldment and/or the heat affected zone (HAZ) in these canisters.

As dictated by the aging management program (AMP), which is required for relicensing applications [1], canister inservice inspection is to be performed. The U. S. Nuclear Regulatory Commission (NRC) requested the Section XI committee of the American Society of Mechanical Engineers (ASME) Boiler and Pressure Vessel Code (BPVC) to provide the requirements for inspection, and Code Case N-860 [2], entitled "Examination Requirements and Acceptance Standards for Spent Nuclear Fuel Storage and Transportation Containment Systems" was undertaken. The code case includes inspection, flaw acceptance standards, and corrosion assessment to manage the potential CISCC degradation. The Code Case N-860, under development since 2015, has been recently board approved in July 2020. Currently it is in preparation for publication by ASME.

An important element of Code Case N-860 is to provide guidance on flaw disposition. This would require an assignment of a crack growth rate (CGR) [3] should a flaw be detected and determined to be due to CISCC. Many CISCC tests under marine environments or various brine conditions have been conducted for several years, including the work done by Savannah River National Laboratory (SRNL). Parallel CISCC testing has been developed at Korea University (KU) under the U. S. Department of Energy (DOE) International Nuclear Energy Research Initiative (I-NERI) between the United States (SRNL) and the Republic of Korea (KU) [4]. These activities and test results have been summarized in a previous report [5].

This report describes the testing in progress at SRNL to investigate CISCC growth behavior using a large plate harvested from the SNL mockup canister. The report provides a brief summary of the series of "big plate" testing performed at Sandia national Laboratories (SNL) to investigate CISCC initiation.

[1] For actual deliquescence, a temperature between 50 to 55 ºC is the maximum possible. However, at 15% RH where SCC has been observed experimentally, the maximum temperature is in the range of 65-70ºC.

The purpose of the SRNL test was to investigate CISCC growth behavior in an as-fabricated canister weldment as driven by WRS. A large section (approximately 51×46 cm with thickness 16 mm and weight about 30 kg), which contains a circumferential weld, was cut from a mockup canister at SNL [6]. Through-wall and part-through-wall (surface) starter cracks, either parallel or perpendicular to the weld, were fabricated with electrical discharge machining (EDM). The stress intensity factor (*K*) for each machined starter crack under canister welding residual stress was estimated by the American Petroleum Institute (API) 579 procedure [7-9]. Dry salt was applied over these machined cracks (estimated 2.3 grams Cl^-/m^2) and natural deliquescence was allowed to take place at room temperature approximately 22 °C and 73% relative humidity (RH) [10,11]. The SRNL large plate test has been in progress since May 2019. No CISCC has been observed, but the evolution of general corrosion in the weld region and the localized corrosion in the immediate vicinities of the starter cracks has been carefully monitored by visual examination and documented. The test will be terminated in May 2021 when the total exposure time reaches two full years. The large plate will be taken out of the test cell and cleaned for nondestructive examination (NDE) to inspect for stress corrosion cracks that might have initiated and grown from the edges of the starter cracks. Then it will be followed by destructive examination by sectioning the selected starter crack regions into thin slices to reveal potential crack growth and crack morphology. If CISCC is found, the average CGR can be estimated and compared with previous CGR test results [5].

2. SAVANNAH RIVER LARGE PLATE DEMONSTRATION TEST

The CISCC for long-term storage of the SNF canisters is investigated at Savannah River Laboratory with a large stainless steel plate (dual certified 304/304L) harvested from the full-size mockup canister at Sandia National Laboratories. The canister plate chemical composition [6] and the tensile properties[2] are shown in Tables 1 and 2, respectively.

Table 1. Material Chemical Composition for Sandia mockup canister (wt.%) [6]

Materials	C		Co	Cr	Cu	Mn	Mo	N	Ni	P	S	Si
Base Metal 304/304L	0.0223		0.1865	18.1000	0.4225	1.7125	0.3180	0.0787	8.0270	0.0305	0.0023	0.2550
Weld Filler Lot 1 308L	0.014		—	19.66	0.16	1.70	0.11	0.058	9.56	0.025	0.010	0.39
Weld Filler Lot 2 308L	0.0012		—	19.71	0.192	1.730	0.071	0.053	9.750	0.024	0.012	0.368

Table 2. Sandia Mockup Canister Plate Tensile Properties (Pre-fabrication)

0.2% Yield Stress	Tensile Strength (UTS)	Elongation in 50.8 mm (2 inch.) Gauge	Reduction in Area (RA)	Hardness (RB)
37.87 ksi 261 MPa	86.6 ksi 597 MPa	62.5%	66.43%	81.5

As shown in Figure 1, the Savannah River large plate was sectioned through a region of the canister that contains a circumferential weld and has a planar dimension of 51×46 cm (20×18

[2] Enos, David G. to Sindelar, R. L., email communication, May 5, 2016 (Attachment: "Weld parameters.xlsx").

inch.) with a thickness of 16 mm (⅝ inch.) and its weight is approximately 30 kg. The objective of the demonstration is to verify the potential for continual crack growth as well as the crack growth characteristics (such as direction and branching, etc.); and if possible, to quantify the averaged CGR and to validate the CGR model [3,5] used to support the development of ASME Section XI Code Case N-860 [2]. The SRNL large plate test was initiated in May 2019.

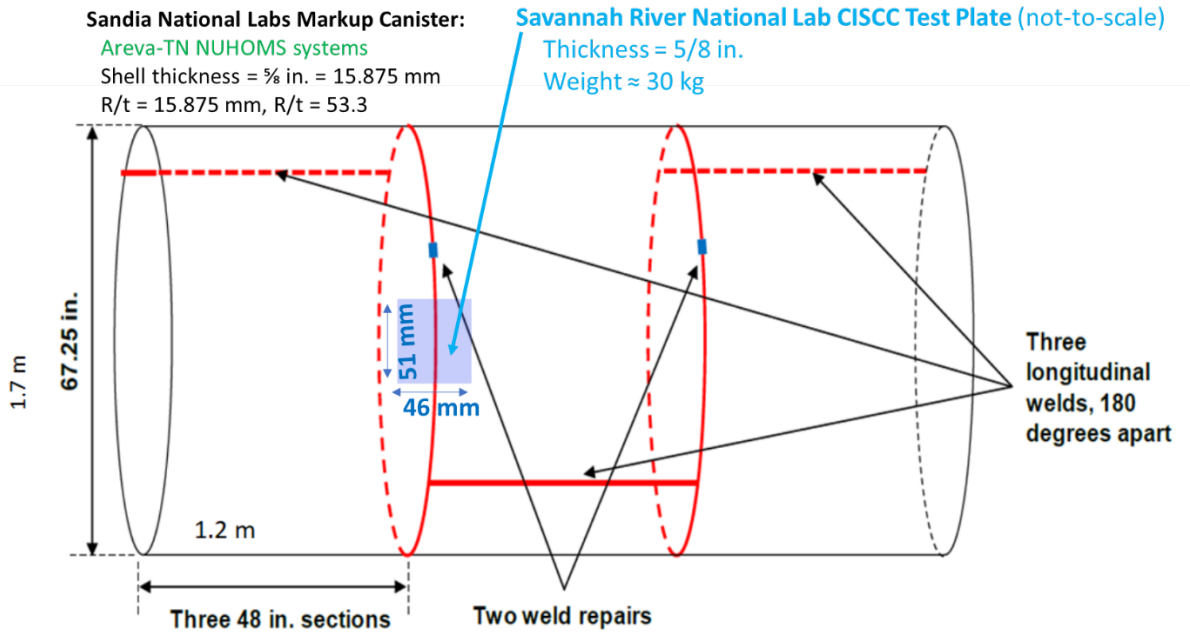

Figure 1. A sketch of the full size mockup canister showing the fabrication welds and the representative location where the SRNL large plate was harvested.

2.1. Welding Residual Stress

The SNF storage and transportation canisters are not required to have post-weld heat treatment after fabrication to relieve the WRS. Under certain corrosive environmental conditions, such as in the chloride-rich coastal regions where the canisters are stored, the WRS could become the mechanical driving force to cause SCC. This phenomenon has been demonstrated in similar large plate tests for welded A285 and A537 carbon steels used to construct the Savannah River high-level nuclear waste tanks [12-14] and the results were consistent with field experience.

To facilitate structural integrity assessment as required in the AMP for SNF canisters, the WRS distributions have been determined experimentally at SNL [6]. For a circumferential weld that is associated with the current Savannah River large plate test, the SNL WRS results are summarized in Figure 2, in which the black curves represent the average of the experimental (measured) values [6], and the red curves are the 4th-order polynomial curve fitting that is needed to facilitate stress intensity factor (SIF) calculations with API 579 [7,8] (or other similar national or international consensus codes for the industry). The 4th-order polynomial fit reported here was obtained by Korea University under DOE I-NERI/USA-ROK program [4]. These residual stresses were also determined using the finite element method [15] by simulating the actual

welding procedure documented in a previous report [6], and are in good agreement with the experimental results. The designations of these welding residual stresses are shown in Figure 3, where RS2 is the WRS component parallel to the weld and tends to open an axial crack, and RS3 is the WRS perpendicular to the weld and is responsible for opening a circumferential crack.

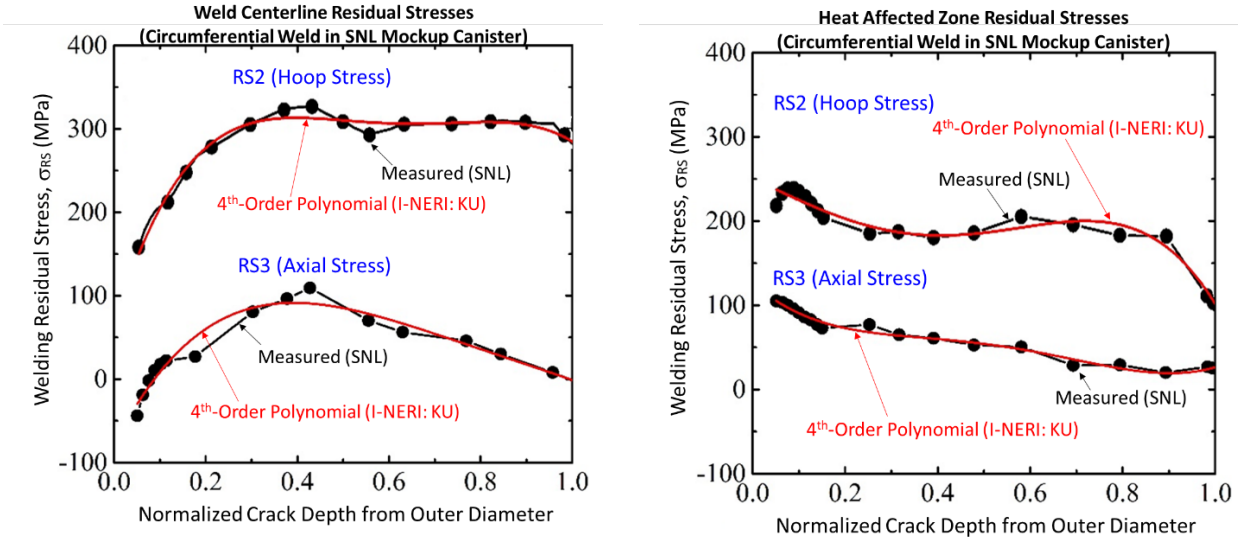

Figure 2. Welding residual stresses associated with the canister circumferential weld. The Weld Centerline and the Heat Affected Zone Residual Stresses were measured at the approximate center of the weld, and at 4 mm from the weld toe (fusion line) into the base material, respectively [6]

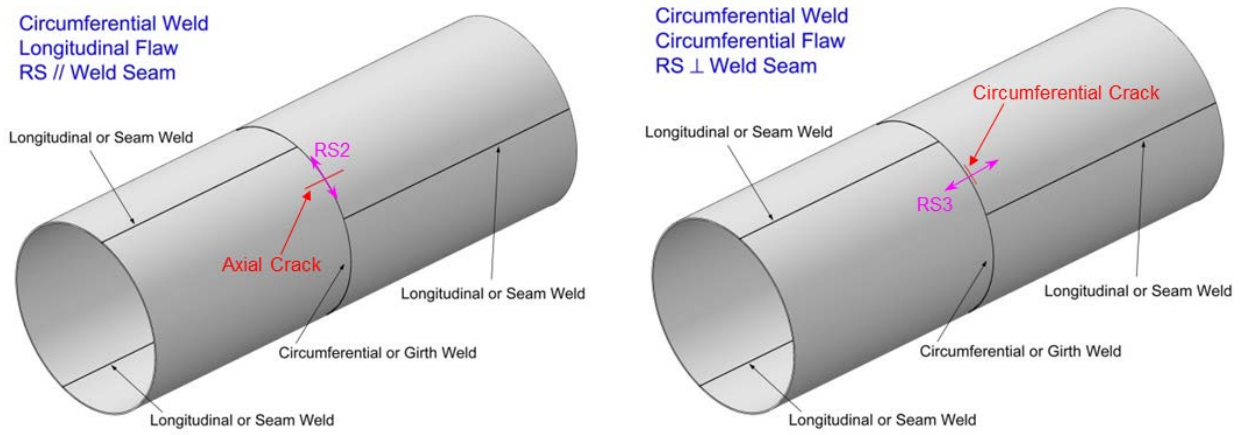

Figure 3. Designations of residual stresses (RS2 and RS3) for a circumferential weld in a canister.

The sizes of the experimental large plates sectioned from the Sandia mockup canister were carefully determined from a series of finite element calculations to minimize WRS redistribution

or relief due to cutting[3]. In a separate study at Oak Ridge National laboratory [16], neutron diffraction was used to determine the remaining WRS in their large plate also from the same mockup canister but with an axial weld. Their experimental data confirmed that most of the as-welded residual stresses were retained in the sectioned plate. Therefore, it is reasonable to assume that the residual stresses in the SRNL large plate were not altered significantly and are similar to those in Figure 2.

2.2. Starter Cracks

Starter cracks (aka seed cracks or machined cracks) were introduced to the large plate in the weld region by EDM. They are intended to create a favorable fracture environment for a stress corrosion crack to initiate and grow under WRS loading. This concept is similar to the fracture toughness test where an initial notch/crack is machined into the specimen (e.g., a compact tension specimen or a single edge notched bend specimen), and it is a standard method to determine the threshold stress intensity factor (K_{ISCC}), below which the SCC is unlikely to occur.

There are seven starter cracks built in the SRNL large plate (Figures 4). The designations and descriptions of these EDM starter cracks are:

Type (a) VT1, VT2: through-wall crack across the weld, crack length = 25 mm;

Type (b) HT1: through-wall crack parallel to the weld edge, crack length = 12 mm;

Type (c) VP1, VP2, VP3: semicircular part-through-wall crack (surface crack) perpendicular to the weld edge, crack length= 12 mm and crack depth = 6 mm;

Type (d) HP1: semicircular part-through-wall crack (surface crack) parallel to the weld edge, crack length= 12 mm and crack depth = 6 mm.

The starter crack layout and orientation is schematically shown in Figure 5. Each type of the EDM crack configuration is shown in Figure 6. When these cracks are overlaid over the contour map of the residual stress parallel to the circumferential weld [6], the WRS loading of these cracks can be seen in Fig. 7. The starter crack tips are located in the weld/HAZ region. Note that the stress contour in Figure 7 only applied to the starter cracks that are perpendicular to the weld (i.e., VT1, VT2, VP1, VP2, and VP3).

[3] Bryan, C. to Sindelar, R. L., email communication, August 14, 2018.

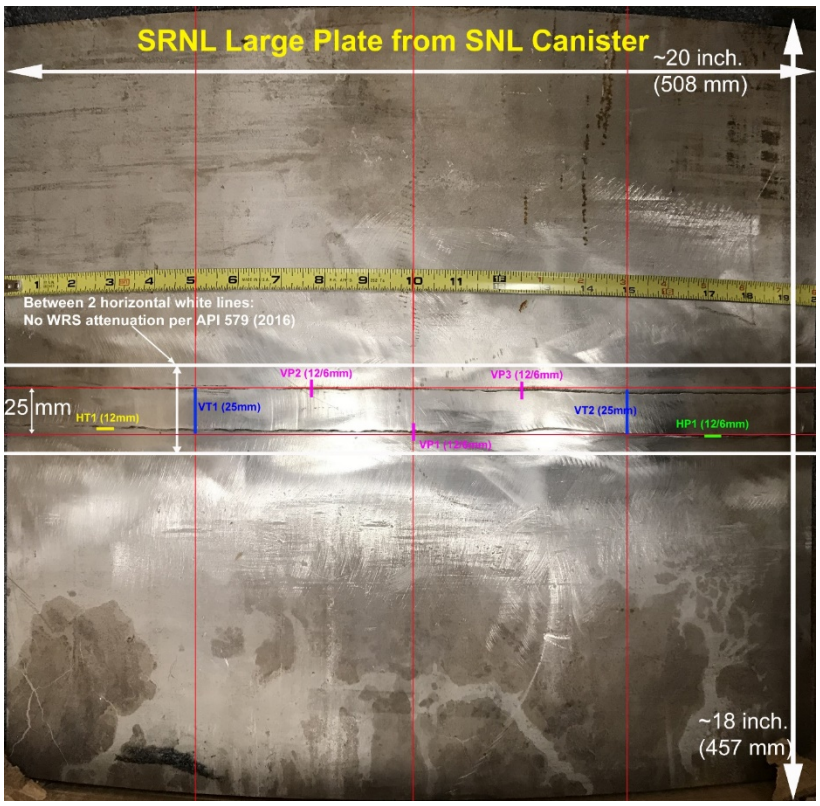

Figure 4. Large plate cut from a canister with an as-fabricated circumferential weld and the locations of starter cracks for CISCC test

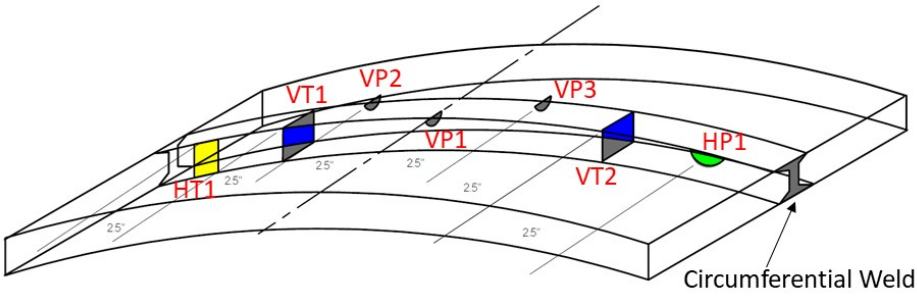

Starter Crack Description (total 7 EDM cracks):

VT1, VT2: Through-wall crack across the weld.
Crack length= **25 mm**

HT1: Through-wall crack parallel to the weld edge.
Crack length= **12 mm**.

VP1, VP2, VP3: Semi-circular Part-through-wall crack perpendicular to the weld edge.
Crack length= **12 mm** and crack depth = **6 mm**

HP1: Semi-circular Part-through-wall crack parallel to the weld edge.
Crack length= **12 mm** and crack depth = **6 mm**

Figure 5. Starter crack layout and orientation in the large plate.

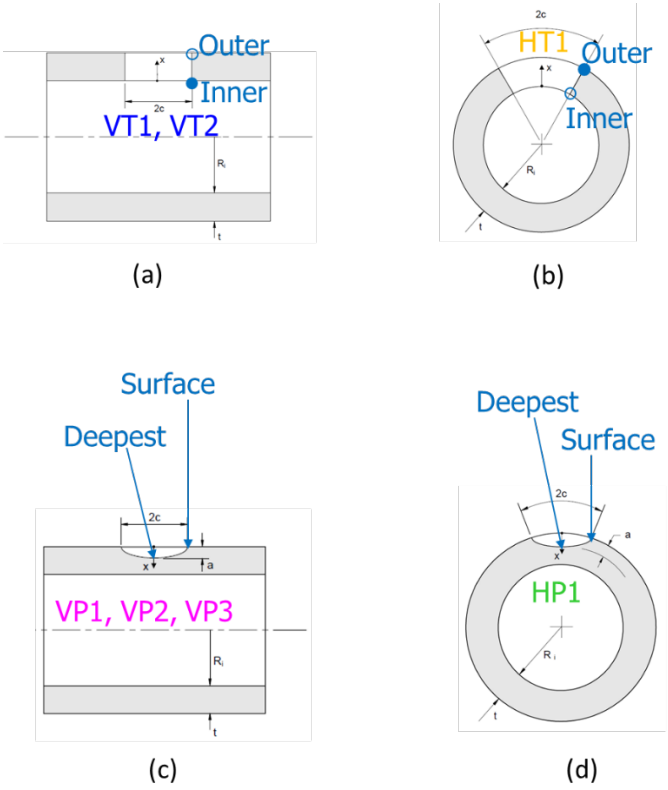

Figure 6. Large plate starter crack configurations: Type (a) VT1, VT2: through-wall crack across the weld; Type (b) HT1: through-wall crack parallel to the weld edge; Type (c) VP1, VP2, VP3: semicircular (*a* = *c*) part-through-wall crack perpendicular to the weld edge; and Type (d) HP1: semi- circular (*a* = *c*) part-through-wall crack parallel to the weld edge

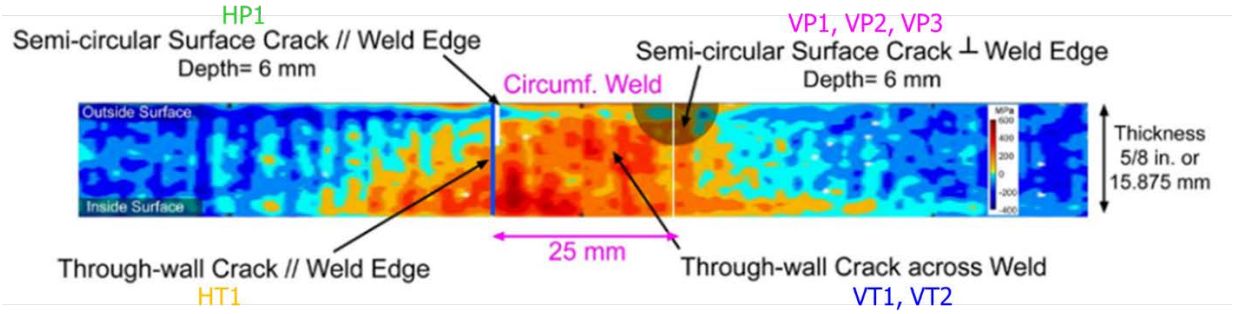

Figure 7. Large plate starter crack design as viewed from plate cross-section through the circumferential weld (superimposed over the contour map for welding residual stress parallel to the weld [6])

The through-wall cracks (VT1, VT2, and HT1) were fabricated with EDM wires of 0.25 mm (0.010 in.) diameter (65% copper and 35% zinc). The resulting width (burn gap) on the plate surface (corresponding to the outer surface of the canister) is approximately 0.43 mm by measurement. For the semicircular, part-through-wall cracks (VP1, VP2, VP3, and HP1),

graphite ram EDM electrodes with width 0.51 mm (0.02 in.) were used. The machined starter crack width on the plate surface is about 0.81 mm.

2.3. Experiment

Artificial sea salt was prepared by following the procedure recommended by ASTM D1141, then deposited on the outer surface of the plate in the welded region with an air brush. The estimated salt load on the plate top surface was 2.3 g/m^2 chloride (dry). The salt coating procedure, as outlined in ASTM G41, "Standard Practice for Determining Cracking Susceptibility of Metals Exposed under Stress to a Hot Salt Environment," was used to create an evenly distributed salt layer over the plate surface. Figure 8 shows the large plate after salt spray and drying, ready for placing inside the test cell.

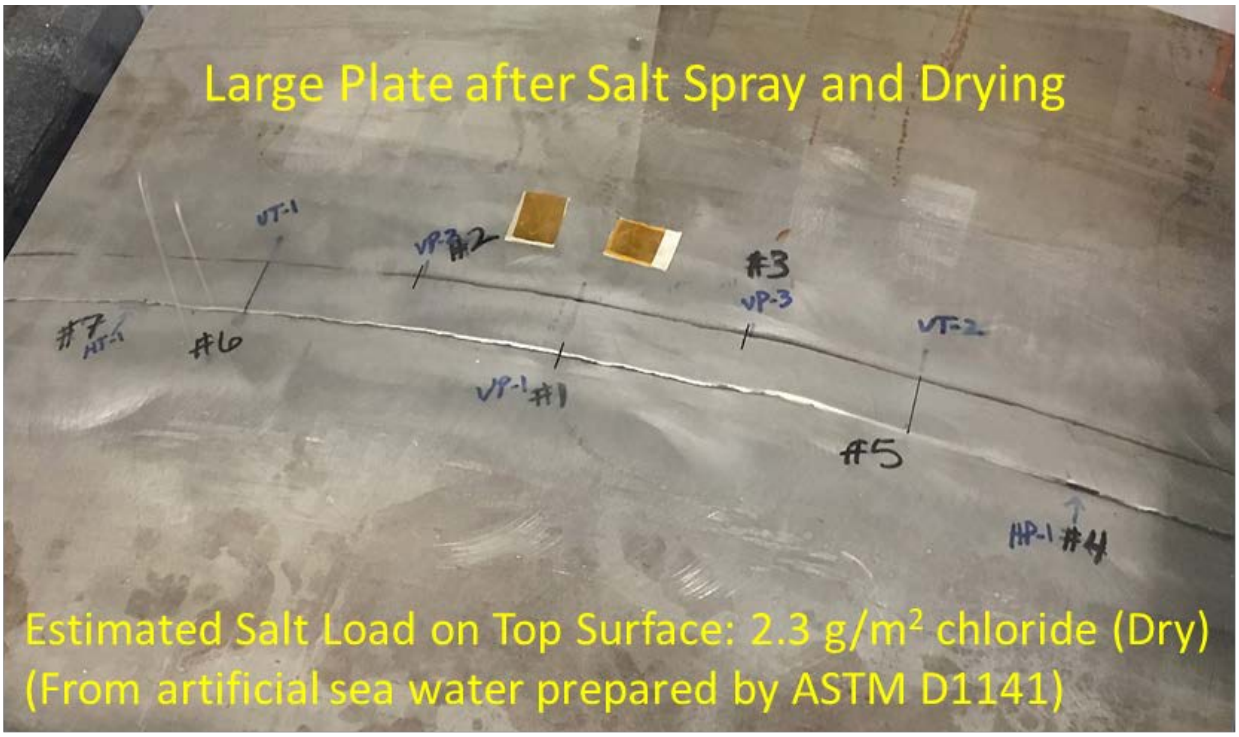

Figure 8. Large plate with EDM starter cracks after salt spray and drying

A transparent polycarbonate (LEXAN™) test cell with an outside dimension of 56×53×15 cm with wall thickness 12.7 mm (0.5 in.) was constructed to house the large stainless steel plate which is supported by a riser over a salt bed with saturated NaCl. Based on ASTM E104, a constant 73% RH environment would be maintained inside the water-tight test cell at room temperature typically 22 °C.

Initially, seven Phased Array Ultrasonic Test (PAUT) wedges and transducers were mounted on the salt-free surface of the plate (or the concave side of the plate corresponding to the inner surface of the canister) for on-line monitoring of crack growth. These sensors have been since removed due to excessive noise preventing satisfactory measurements. Figure 9 illustrates the overall experimental setup and Figure 10 shows the closeup of the salt tray that is used to maintain a constant RH environment by following ASTM E104, "*Standard Practice for Maintaining Constant Relative Humidity by Means of Aqueous Solutions*."

The large plate is currently being exposed to a CISCC environment in 73% RH at room temperature (~22 °C) since May 2019.

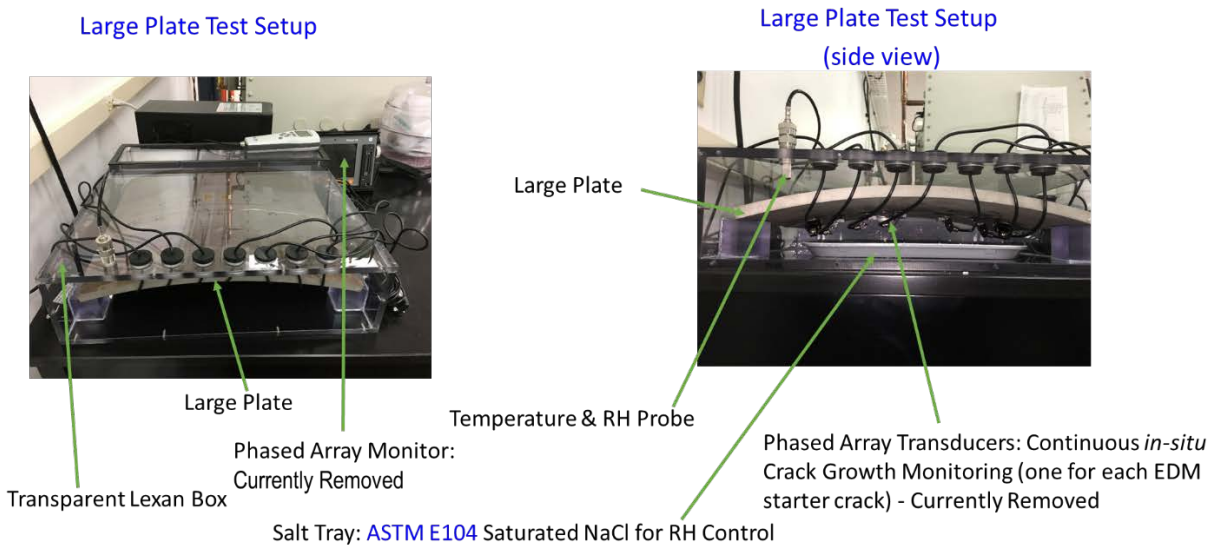

Figure 9. Experimental setup of the large plate CISCC test under naturally deliquescing sea salt at room temperature and 73% RH (PAUT wedges have been removed)

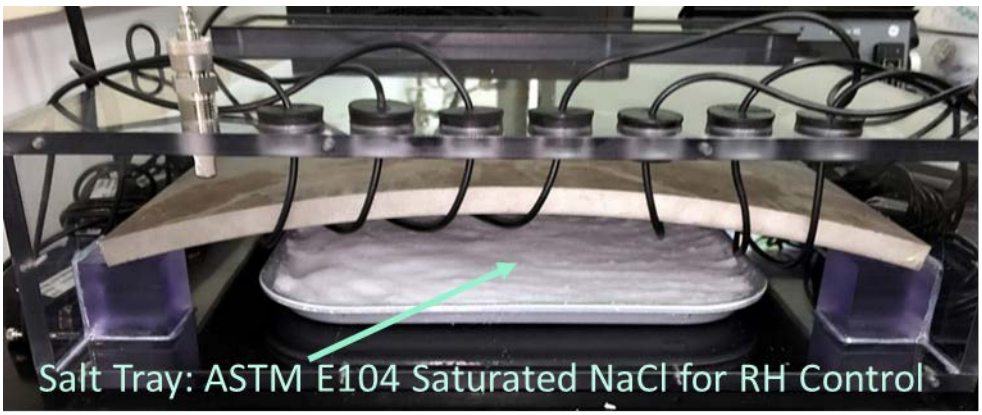

Figure 10. The NaCl salt tray under the large plate for maintaining a constant relative humidity in the test cell.

2.4. Experimental Observations

The test was initiated on May 8, 2019. As reported previously [5], the temperature and RH reached equilibrium quickly. The initially dry salt film originally covered the plate surface turned into numerous liquid droplets in a few hours, similar to the "big plate" tests conducted at Sandia National Laboratories (Section 4). This indicated that the natural deliquescence has taken place.

2.4.1. Initial Exposure (5 Months)

The SRNL large plate test has been periodically examined for CISCC and documented with digital images for each starter crack. The evolution of the starter cracks and their immediate vicinities, observed from May 9 to October 16, 2019, is shown in Figure 11. It can be seen that the general corrosion is progressively developed, especially along the weld and the base metal interface. No SCC has been observed at the started cracks or elsewhere on the plate.

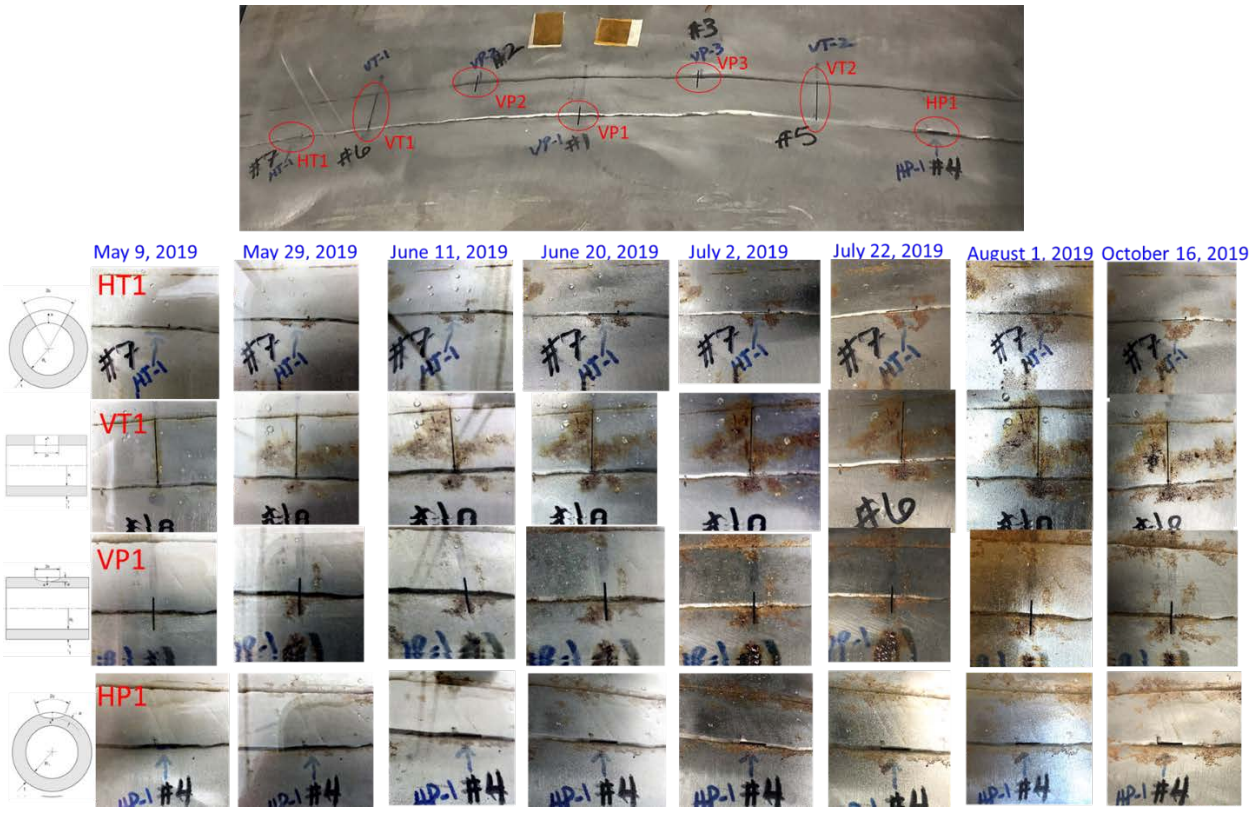

Figure 11. Evolution of chloride-induced corrosion near starter cracks during 5 months of exposure at room temperature about 22C and 73% RH

2.4.2. Test Augmented with Elevated Chloride Concentration

Because no cracking was observe after 5 months of exposure with the initial salt load of 2.3 grams Cl^-/m^2 on the plate surface, two starter cracks (VP2 and HP1) were selected to receive additional salt load, where VP2 is a semicircular surface crack perpendicular to the weld, and HP1 is a semicircular surface crack parallel to the weld edge. The original crack lengths are both 12 mm on the plate surface. As seen in Figure 12, these two cracks were isolated with putty material (yellow) from the other starter cracks and the extra salt was applied to the enclosed areas on October 24, 2019). The deliquesced salt brine droplets can be seen in Figure 12.

Figure 12. Additional salt applied to selected starter cracks (VP2 and HP1).

Figure 13 shows the corrosion activities of VP2 from October 16, 2019 (about a week before the extra salt was applied) through March 25, 2020. Most of the corrosion products appear to be highly concentrated with iron. A very small spot with light-colored, crack-like morphology seemed to form at the lower crack tip across the crack opening, but it may be just a small salt cake or crystal that has been broken up. This will be further investigated after the test is complete in May 2021.

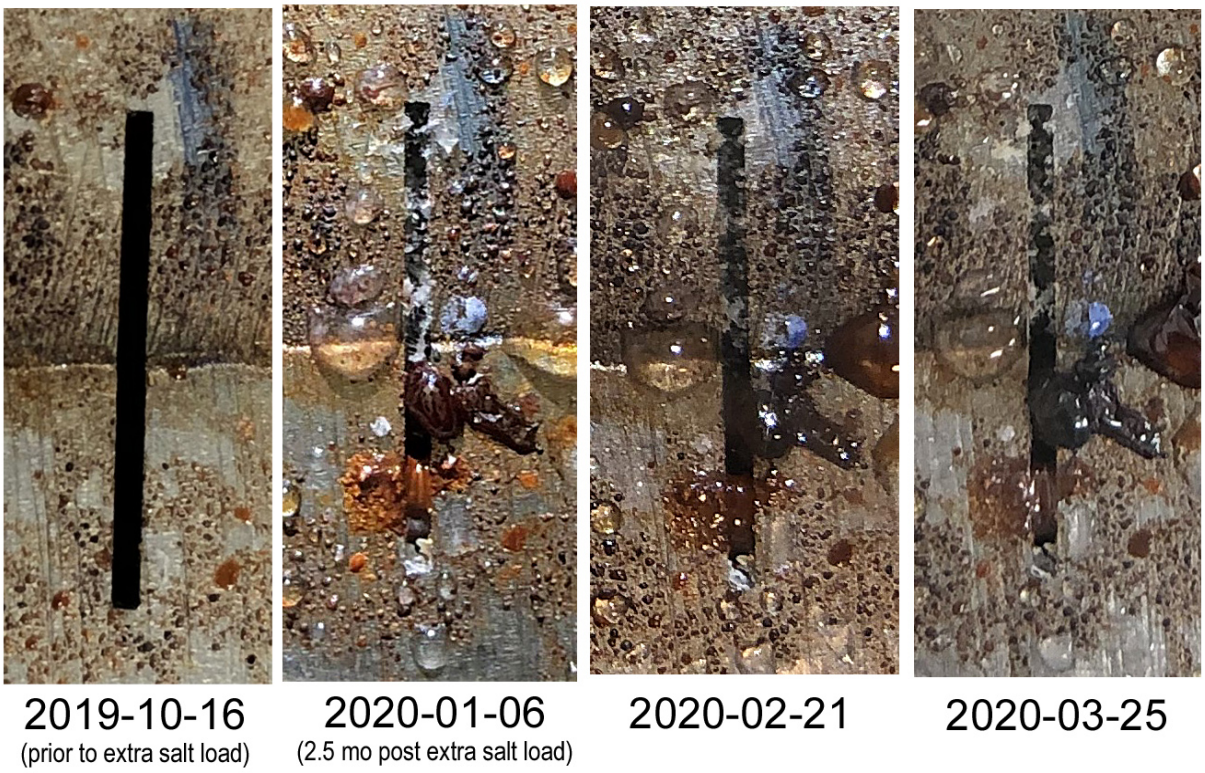

Figure 13. Closeup view of corrosion evolution of a semicircular surface crack VP2 after additional salt was applied (original crack length is 12 mm and is perpendicular to the weld)

2.4.3. Evolution of General Corrosion

A comparison of general corrosion in the weld region across the width of the entire large plate from May 9, 2019 (test initiation date) through February 21, 2020 is shown in Figure 14. It can be seen that the corrosion pattern appears to be stabilized quickly (sometime between May and October 2019). Even with extra salt applied to two of the starter cracks on October 2019, it seems that the appearance of general corrosion was not affected (Figure 14). Of course, in the very close vicinities around those two starter cracks with extra salt load, the corrosion remains relatively active (see VP2 in Figure 13).

Figure 14. Evolution of general corrosion on the large plate in weld region

2.5. Propensity of CISCC in Large Plate with Starter Cracks

The Mode I stress intensity factor (K_I) is typically used as an indication for an existing crack whether it will grow in tensile opening mode under the external or internal loads. In the case of SCC, a threshold stress intensity factor, K_{ISCC}, may exist, such that crack growth can only take place when $K_I \geq K_{ISCC}$. The value of K_{ISCC} is experimentally determined and it is regarded as an environmentally dependent material property.

2.5.1. Stress Intensity Factor Calculation Procedure

For the current SRNL large plate testing under an exposure condition at room temperature of 22 °C and 73% RH with 2.3 grams Cl^-/m^2 of salt on the plate surface, the only loading is the welding residual stresses due to fabrication of the canister. No external loads are applied. Note that for a circumferential weld as in this large plate, only the WRS parallel to the weld (RS2) and that perpendicular to the weld (RS3) are relevant. The API 579 Fitness-for-Service procedure is used to evaluate stress intensity factor K_I for each of the starter crack (see Figures 4-8): The first step is to approximate the measured through-thickness WRS by a 4th order polynomial, then apply the coefficients of the 4th-order polynomial to the API equations in Annex C of the 2007 edition [7] or Annex 9C in the 2016 edition [8]. The detailed procedure is described below.

(1) Curve fitting of the fourth-order polynomial
Equation (1) is used to curve fit the WRS (σ) measured by Sandia National Laboratories [6] (see Figure 2):

$$\sigma(x) = \sigma_0 + \sigma_1\left(\frac{x}{t}\right) + \sigma_2\left(\frac{x}{t}\right)^2 + \sigma_3\left(\frac{x}{t}\right)^3 + \sigma_4\left(\frac{x}{t}\right)^4 \quad (1)$$

where σ_i (i=0 to 4) are the coefficients of the 4th-order polynomial, t is the canister wall thickness, and x is the through-wall coordinates with x= 0 at the inside dimeter (ID) of the canister for through-wall cracks or x=0 at the outer diameter (OD) for the outside part-though-wall surface cracks (see the coordinate system in Figure 6, or its definition in API 579 [7,8]). The values of σ_i have been determined by Korea University under I-NERI/USA-ROK program [4] and are listed in Table 3.

Table 3. Coefficients of the 4th-Order Polynomial to Approximate Welding Residual Stress

Seed Crack	Crack Location	x=0 Location	σ_0 (MPa)	σ_1 (MPa)	σ_2 (MPa)	σ_3 (MPa)	σ_4 (MPa)
VT1, VT2	WCL	ID	283	347	-1701	3310	-2169
	HAZ		100	902	-2746	3136	-1142
VP1, VP2, VP3	WCL	OD	69	1803	-4787	5367	-2169
	HAZ		249	-249	-191	1432	-1142
HT1	WCL	ID	-1	191	-80	361	-550
	HAZ		27	-162	1077	-1751	936
HP1	WCL	OD	-79	1086	-2298	1840	-550
	HAZ		127	-484	1442	-1994	936

WCL: Weld Centerline
HAZ: Heat Affected Zone

Seed Crack Description:
VT1, VT2: Through-wall crack, longitudinal direction, perpendicular to circumferential weld.
VP1, VP2, VP3: Surface crack on outer diameter, longitudinal direction, perpendicular to circumferential weld.
HT1: Through-wall crack, circumferential direction, parallel to circumferential weld.
HP1: Surface crack on outer diameter, circumferential direction, parallel to circumferential weld.

(2) Stress intensity factor calculation:
As outlined by the API 579-1/ASME FFS-1 [7,8], the stress intensity factor for a through-wall crack in a cylindrical shell structure (such as VT1, VT2, or HT1) is expressed by

$$K_I = \left[\{\sigma_m + p_c\}G_0 + \sigma_b\left(G_0 - 2G_1\right)\right]\sqrt{\pi c}$$

where σ_m is the membrane stress component of the loading, σ_b is the bending stress component, p_c is the crack face pressure and is zero in the current large plate case, and the influence coefficients G_0 and G_1 are tabulated in API 579 [7,8] for each crack orientation (axial or circumferential) and are a functions of t/R_i (i.e., the ratio of canister wall thickness to canister inside radius). For the equivalent membrane and bending stresses in terms of the 4th-order polynomial formulation:

$$\sigma_m = \sigma_0 + \frac{\sigma_1}{2} + \frac{\sigma_2}{3} + \frac{\sigma_3}{4} + \frac{\sigma_4}{5}$$

$$\sigma_b = -\frac{\sigma_1}{2} - \frac{\sigma_2}{2} - \frac{9\sigma_3}{20} - \frac{6\sigma_4}{15}$$

For a part-through-wall crack without (local) crack face bending, such as the starter crack VP1, VP2, VP3, or HP1, the general expression in API 579 [7,8] is

$$K_I = \left[G_0\left(\sigma_0 + p_c\right) + G_1\sigma_1\left(\frac{a}{t}\right) + G_2\sigma_2\left(\frac{a}{t}\right)^2 + G_3\sigma_3\left(\frac{a}{t}\right)^3 + G_4\sigma_4\left(\frac{a}{t}\right)^4\right]\sqrt{\frac{\pi a}{Q}}$$

Again, σ_i (i=0 to 4) are the coefficients of the 4th-order polynomial, p_c is the crack face pressure and is zero in the current large plate case, and G_i (i=0 to 4) are influence coefficients that are tabulated in API 579 [7,8] for each crack orientation (axial or circumferential) and are functions of t/R_i, a/c, and a/t (c is the half crack length of the semi-elliptic surface crack, a is the crack depth, and t is the canister shell thickness).

2.5.2. Stress Intensity Factor Calculation Results

Both sets of welding residual stresses at the weld centerline (WCL) and at the HAZ (Figure 2) were used in calculating stress intensity factors. The experimental data were obtained at Sandia National Laboratories [6] and the 4th-order polynomial curve fitting was performed at Korea University [4].

The SIF solutions for the through-wall axial starter cracks across the circumferential weld (VT1 and VT2) are tabulated in Table 4, and are labelled in Figure 15 at the crack tips where they were calculated. The contour map in Figure 15 represents the WRS parallel to the weld [6]. This stress component is responsible for opening the starter cracks VT1 and VT2. Figure 15 also includes the actual images of VT1 and VT2 after 9 months of exposure. Stress corrosion cracking has not been observed at the crack tips.

Table 4. Stress Intensity factors for starter cracks VT1 or VT2 (Axial through-wall crack: Half crack length *c* = 12.5 mm)

Welding Residual Stress	Crack Tip Location	Stress Intensity Factor (MPa√m)
Weld Centerline	Outside Surface	51.6
	Inside Surface	64.3
Heat Affected Zone	Outside Surface	46.1
	Inside Surface	33.3

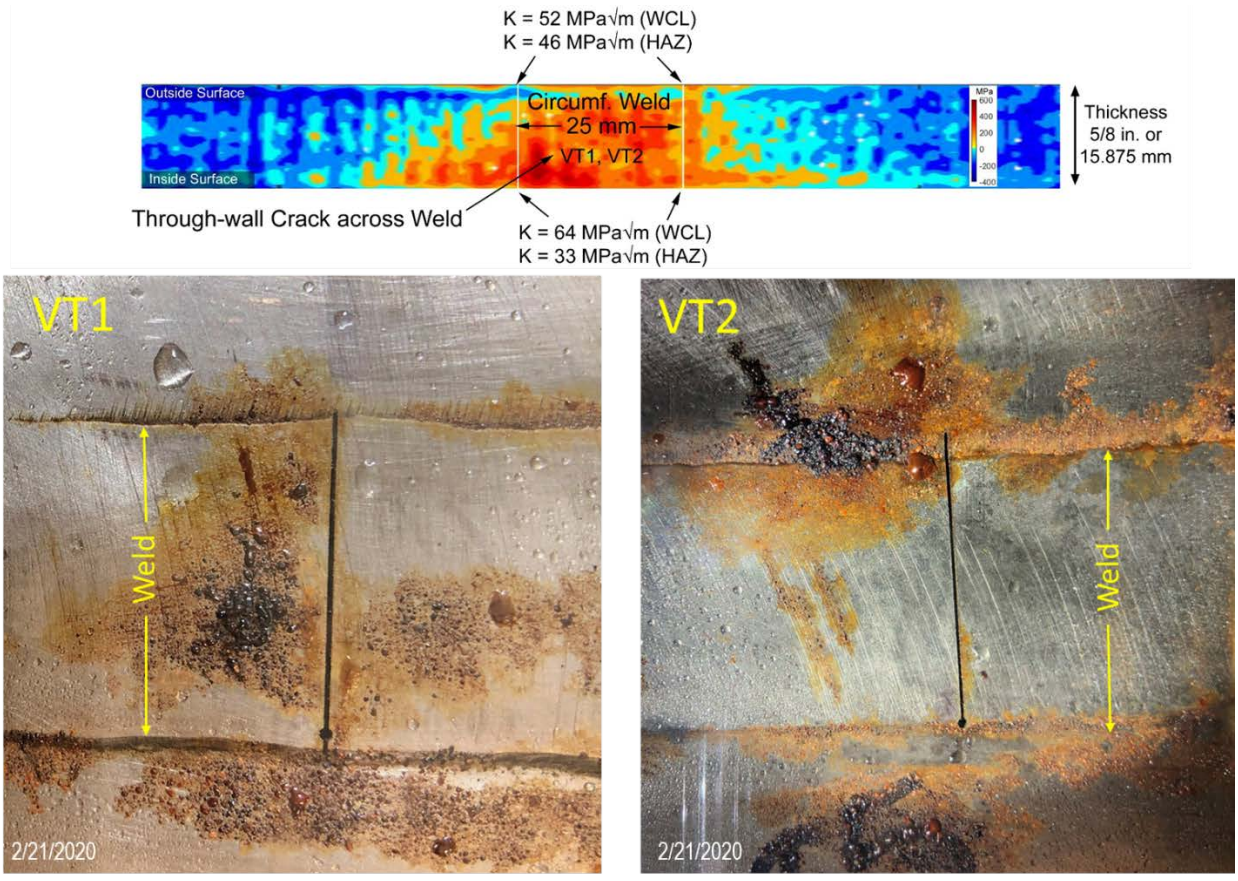

Figure 15. Stress intensity factor solutions for the starter crack VT1 or VT2 and the images of these cracks after 9.5 months of exposure (VT1 and VT2 are through-wall cracks across the weld).

Likewise, the SIF solutions for the part-through-wall axial surface cracks perpendicular to the weld (VP1, VP2, and VP3) are tabulated in Table 5 and labelled in Figure 16. The images after 9months of exposure condition can also be seen in Figure 16. For starter cracks parallel to the weld (HP1: part-through-wall and HT1: through-wall), their SIF solutions are tabulated in Tables 6 and 7 and labelled in Figure 17, which also shows the starter crack images after 9 months of exposure. Stress corrosion cracking has not been observed for any of the starter cracks.

Table 5. Stress Intensity factors for starter cracks VP1, VP2, or VP3 (Axial surface crack: Half crack length *a* = Crack depth *c* = 6 mm; Semicircular)

Welding Residual Stress	Crack Tip Location	Stress Intensity Factor (MPa√m)
Weld Centerline	Deepest Point	26.0
	Surface Point	16.9
Heat Affected Zone	Deepest Point	18.3
	Surface Point	26.4

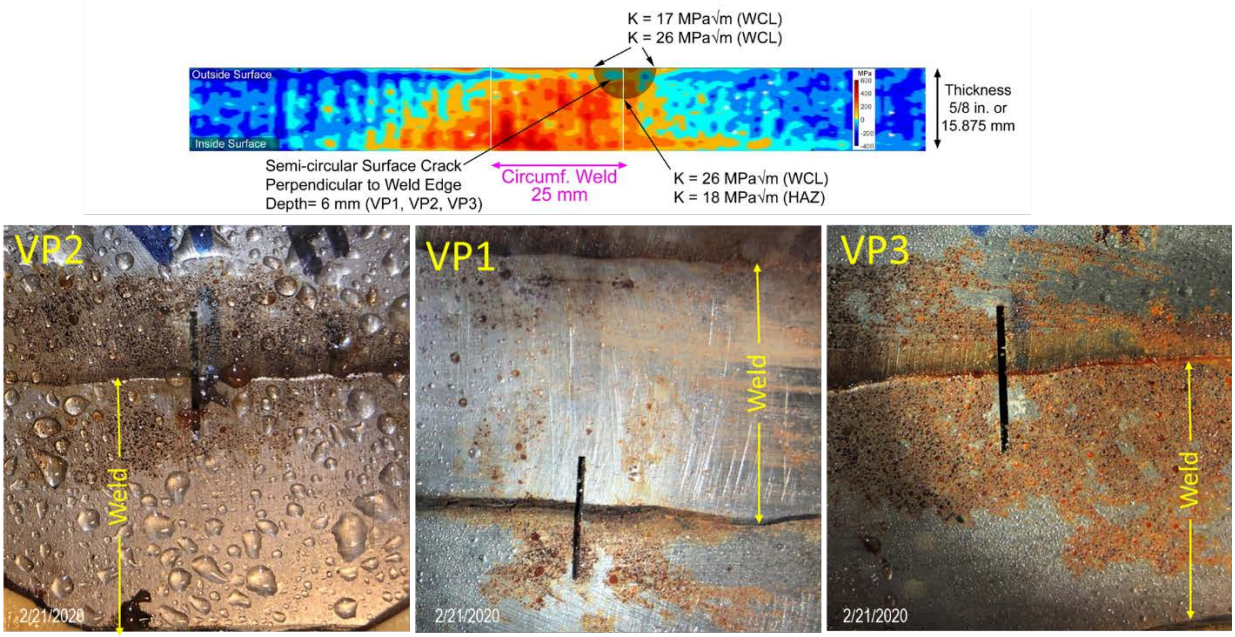

Figure 16. Stress intensity factor solutions for the starter crack VP1, VP2, or VP3 and the images of these cracks after 9.5 months of exposure (VP1, VP2, and VP3 are semicircular part-through-wall surface cracks perpendicular to the weld).

Table 6. Stress Intensity factors for starter crack HP1
(Circumferential surface crack: Half crack length *a* = Crack depth *c* = 6 mm; Semicircular)

Welding Residual Stress	Crack Tip Location	Stress Intensity Factor (MPa√m)
Weld Centerline	Deepest Point	5.6
	Surface Point	-3 (Crack Tip Closure)
Heat Affected Zone	Deepest Point	7
	Surface Point	12

Table 7. Stress Intensity factors for starter cracks HT1
(Circumferential through-wall crack: Half crack length *c* = 12 mm; Semicircular)

Welding Residual Stress	Crack Tip Location	Stress Intensity Factor (MPa√m)
Weld Centerline	Outside Surface	6.5
	Inside Surface	6.7
Heat Affected Zone	Outside Surface	13.3
	Inside Surface	1.9

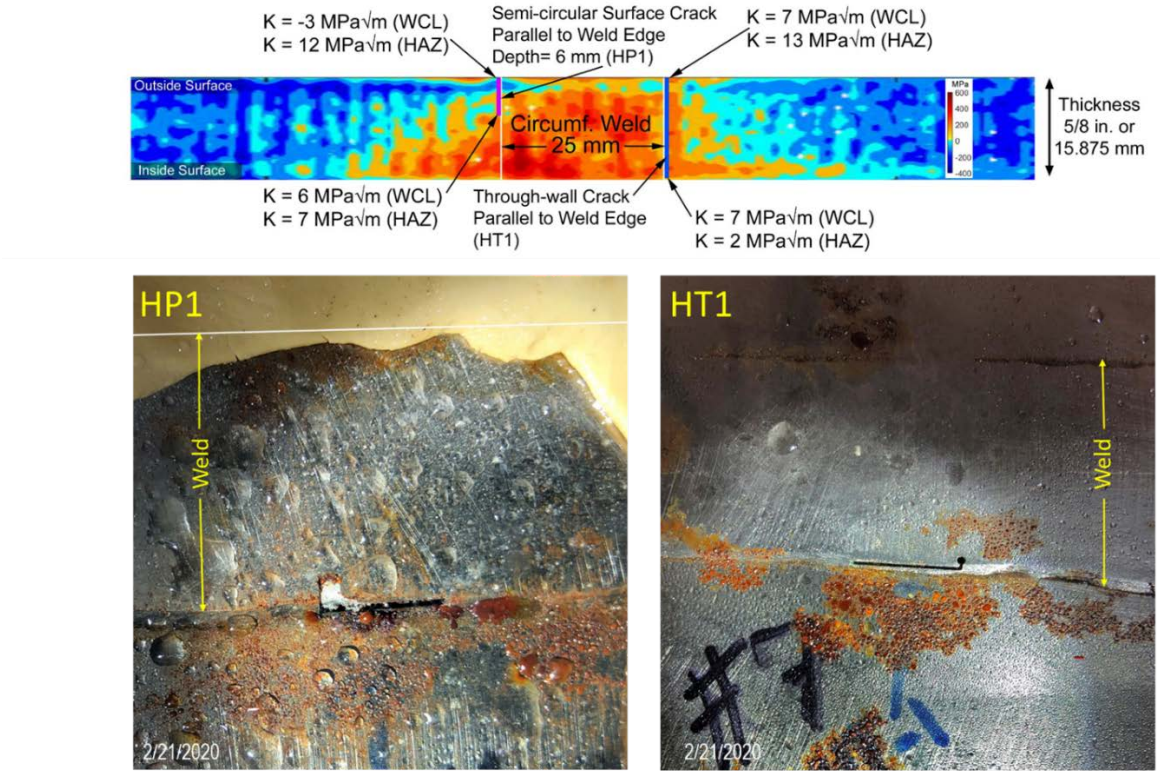

Figure 17. Stress intensity factor solutions for the starter cracks HP1 and HT1, and the images of these cracks after 9.5 months of exposure (HP1 is a semicircular part-through-wall surface cracks parallel to the weld; and HT1 is a through-wall crack parallel to the weld).

2.5.3. Propensity of CISCC in Large Plate Test

This section uses existing experimental data of CGR for typical SNF canister stainless steels in chloride-rich environments to provide insight and expectation for the SRNL large plate test.

Natural exposure tests for stainless steels 304, 304L, and 316(LN) were conducted on Miyakojima (Miyako Island), which is one of the most corrosive areas in Japan [17,18]. Three-point bend specimens with thickness of 10 mm, each containing either a 3 mm deep part-through-plate precrack across the width, or a 3mm deep semicircular surface precrack. The specimens were loaded to 0.4 or 0.8 proof stress (PS). Both direct exposure and under glass method were used with average sample surface temperatures at 26.7 and 26.6 °C, respectively. The average relative humidity on the island is 80% (varying between 73% in January and 86% in June [19]). As seen in Figure 18, the experimentally determined CGRs for Type 304 base metal and weld were approximately in the order of 6×10^{-12} m/s, with the K_I loading range between 0.6 to 9 MPa√m.

Accelerated tests were also conducted for the base metal and weld of Type 304 stainless steel by Kosaki [17,18] at 60 °C and 95% RH using the same specimen design as in the Miyakojima natural exposure tests. The specimens were exposed to NaCl steam mist environment with saturated NaCl concentrated on the specimen surface. The resulting CGRs for Type 304 base metal using semicircular precracked specimens are about 9.3×10^{-10} m/s [17,18] and the SIF loading range is between 2 and 20MPa√m[4], as shown in Figure 19. Also included in Figure 19 are the recent Korea University test data using S30400 stainless steel [21,22]. The test results were obtained by immersing the specimens in 5 % salinity artificial seawater at 50 °C. Because standard ASTM compact tension specimens were used in the KU tests, higher SIF loading was achieved and K_I was between 15.3 and 23.2 MPa·√m, as shown in Figure 19. The CGRs determined from the immersion test at 50 °C are about 1×10^{-10} m/s, which is one order of magnitude less than the Kosaki data obtained at 60 °C. For comparison purpose, the S31603 test data obtained by Tani et al. [23] at 50 °C and 35% RH are also included in Figure 19. As expected, the CGR for S31603 is much lower and is in the order of 1×10^{-12} m/s, which clearly shows the alloy effect.

From the results plotted in Figures 18 and 19, it can be concluded that the CGR from accelerated test at 50 °C is two orders of magnitude faster than the natural exposure condition at 27 °C. All the test data collectively indicate that CGR appears to be insensitive to the SIF, and CISCC can take place at a small threshold value (K_{ISCC}) even below 1 MPa√m. For the SRNL large plate test, Section 3.4.2 shows that the SIF calculated at the starter crack tips are in general higher than the load levels used in Kosaki tests (Figures 18 and 19). Therefore, it is expected that SCC in the SRNL large plate should have taken place. The reasons that no crack growth was observed could be that (i) the WRS may be altered or redistributed due to sectioning of the full size canister into the SRNL large plate and then by fabricating the EDM starter cracks; (ii) the crack

[4] The entire load range (K_I) in Kosaki accelerated tests for all specimen types is 0.3 to 32 MPa√m. Figure 19 only shows the data from semicircular specimens.

growth is still under the incubation phase; and (iii) the naturally deliquescing salt on the large plate surface did not reach the machined crack fronts.

The crack initiation tests were also conducted by Kosaki [18]. Thin (1.5 mm in thickness) but non-cracked specimens were tested with four-point bend under the same natural exposure and accelerated test conditions [17,18]. Only Type 304 test data from the natural exposure (average 27 °C and 80% RH) with 1.0 PS loading are used for discussion here, because the exposure condition is similar to the large plate test (nominally 22 °C and 73% RH) and the WRS could be at 1.0 PS level. The Kosaki data show that at least 993 and 364-573 days are required for a stress corrosion crack to initiate in the base metal and weld, respectively. Here the more conservative data obtained from the under glass method are referenced. Therefore, the Kosaki experiments seemed to imply that, even though the WRS is sufficient to cause stress corrosion crack growth, the incubation time could take as long as a year.

Note that the loadings used in Kosaki initiation tests with four-point bend specimens were 0.5 and 1.0 PS; and the loadings in his three-point bend CGR tests were 0.4 and 0.8 PS. Given the 0.2% yield stress of the mockup canister is 261 MPa (Table 2), the maximum welding residual stresses measured from the Sandia mockup canister (Figure 2) are summarized in Table 8. It can be seen that the WRS levels in the mockup canister are similar to the loading levels that were applied to the Kosaki specimens. Therefore, the Kosaki results on CGR and crack initiation [17,18] may be relevant to the current large plate testing.

Table 8. Maximum welding residual stress measured from Sandia mockup canister

Location of WRS	WRS Component (see Figure 3)	Location of Max. Stress (see Figure 2)	Maximum Stress (1.0 PS = 261 MPa)
Weld Centerline	RS2 (WRS // Weld)	6 mm from OD	330 MPa (1.25 PS)
	RS3 (WRS ⊥ Weld)	7 mm from OD	110 MPa (0.42 PS)
Heat Affected Zone	RS2 (WRS // Weld)	1 mm from OD	210 MPa (0.80 PS)
	RS3 (WRS ⊥ Weld)	1 mm from OD	110 MPa (0.42 PS)

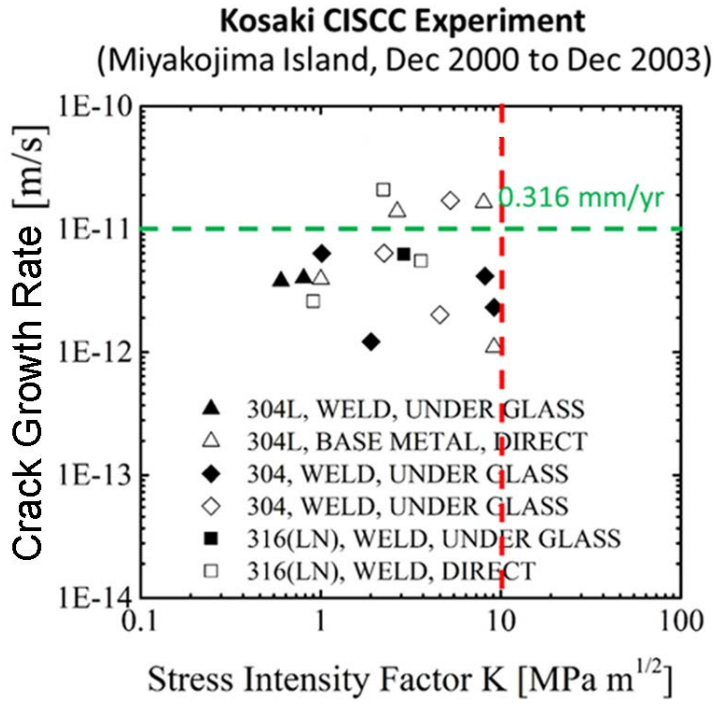

Figure 18. Crack growth rates from natural exposure on Miyakojima [17,18] (Courtesy of Korea University under I-NERI/USA-ROK)

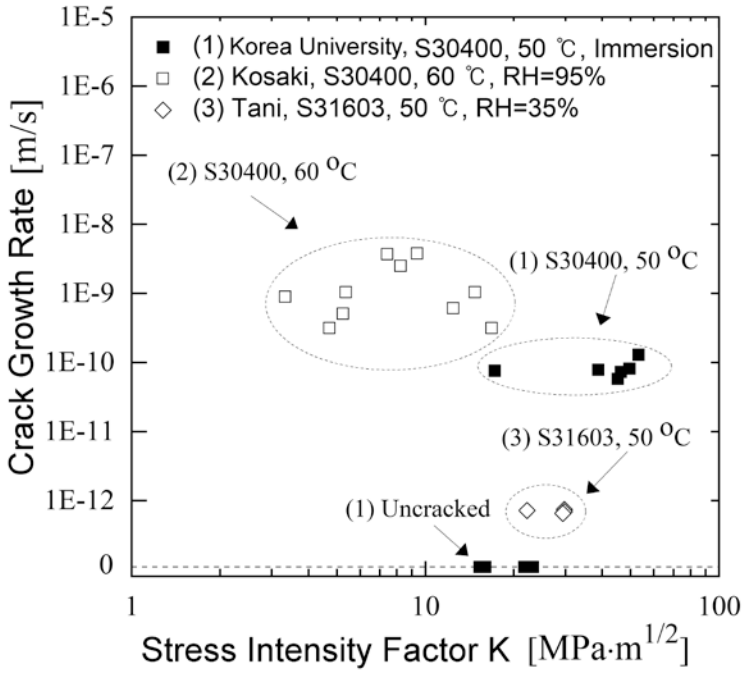

Figure 19. Crack growth rates from laboratory tests for stainless steels at 50 and 60°C under various CISCC conditions [22].

3. SANDIA NATIONAL LABORATORIES "BIG PLATE" TEST

Sandia National Laboratories also harvested several "big plates" containing welds from the mockup canister [24]. Their tests were designed to determine the orientation and location of SCC around canister welds (axial, circumferential, and weld joint) and to evaluate brine evolution under corrosion. Starter cracks were not used in these big plates

The Sandia big plates were pre-loaded with 8 g/m^2 $MgCl_2$. Similar to the SRNL large plate, the salt deliquesced and formed brine droplets as shown in Figure 20. These big plates were then exposed to 80 ºC at 35 % RH for 12 months. The plates were taken out of the ovens after 2 months for visual inspection. It was found that they were heavily corroded but were still damp. The pre- and post-exposure conditions of a plate with a weld joint and a plate with a circumferential weld are shown in Figures 21 and 22. One of the plates was used for detailed examination, but no stress corrosion cracks were found. The other specimens were returned to the ovens and continued the exposure at 80ºC and 35 % RH. After 8 months of testing, the plates were found to be dry and the corrosion products were mostly loose and non-adherent, but covered the entire plate surface. The plates remained in the oven for additional months to complete the 12-month test. The surface deposits were then collected for analysis, and the cleaned plates were subject to NDE, including fluorescent dye penetrant, ultrasound phased array, and eddy current tests. No cracks were detected after 12 months of exposure.

A separate big plate containing a circumferential weld was also loaded with 8 g/m^2 $MgCl_2$ with 3 % Potassium Tetrathionate ($K_2O_6S_4$) at pH =1 for 6 months (with 3 months at 40ºC). NDE was performed but no cracks were found.

Figure 20. Magnesium chloride (8 g/m2 $MgCl_2$) deliquesced and formed brine droplets on a Sandia big plate containing an axial weld.

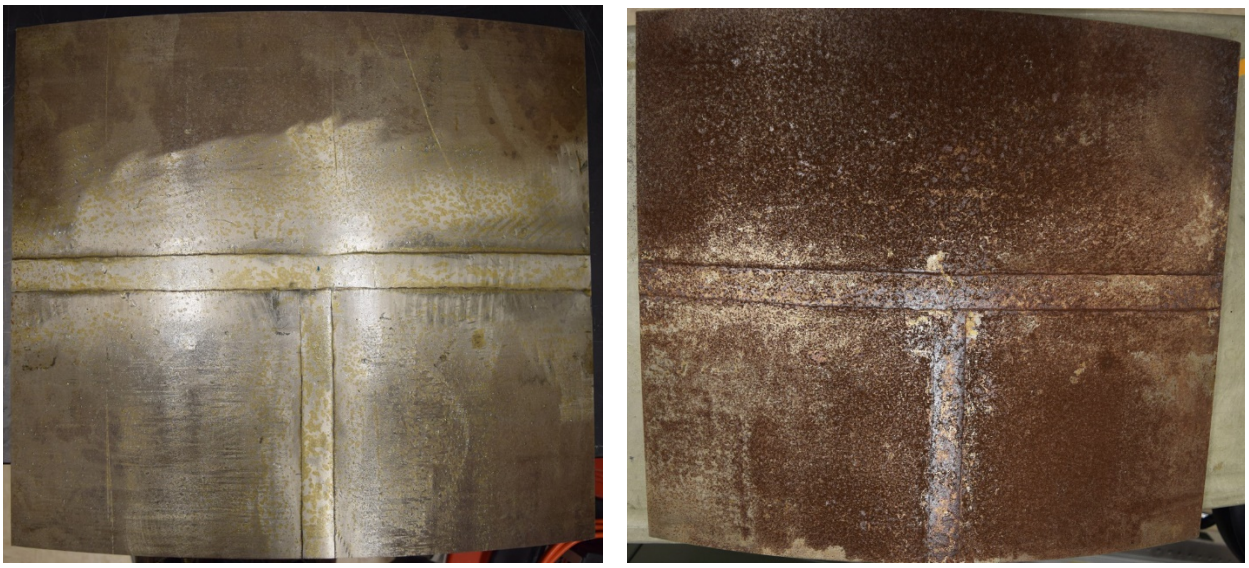

(a) (b)

Figure 21. Sandia big plate containing a weld junction was exposed to 8 g/m2 MgCl2 at 80 ºC and 35 % RH: before exposure (a) and after 2 months of exposure (b).

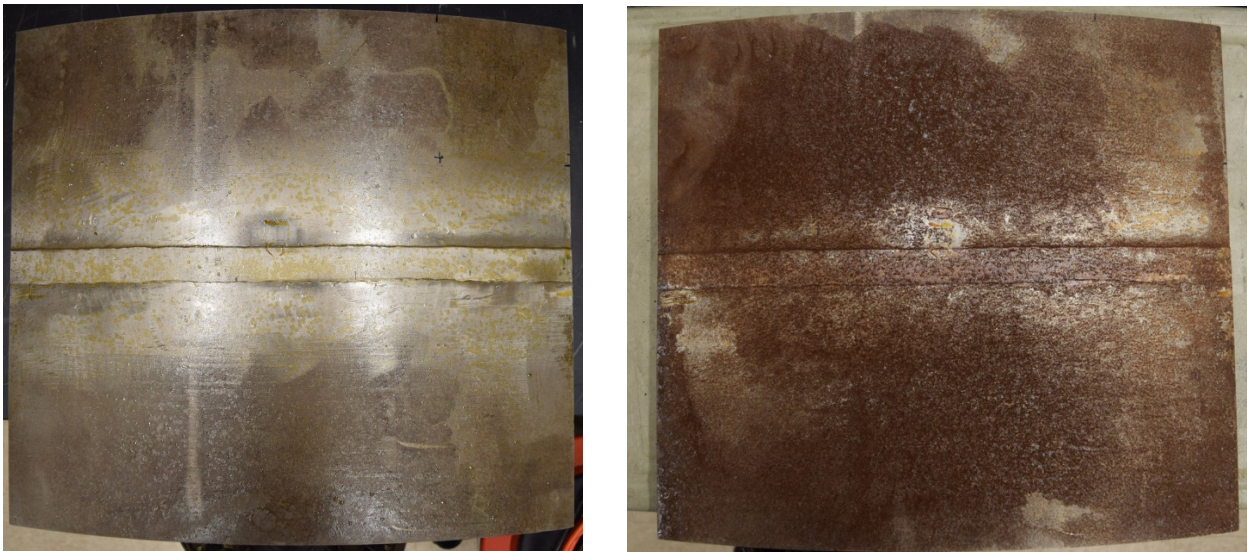

(a) (b)

Figure 22. Sandia big plate containing a circumferential weld was exposed to 8 g/m2 MgCl2 at 80 ºC and 35 % RH: before exposure (a) and after 2 months of exposure (b).

In addition, a four-point bend load frame was built at Sandia National Laboratories. Figure 23 shows that a test specimen of 12.7 mm (0.5 in.) thick, 101.6 mm (4 in.) wide, and 355.6 mm (14 in.) in length (span) was machined and loaded to approximately 200 MPa. The test assembly was transferred to an environmental chamber with the same exposure condition as the big plate

test previously discussed (at 80ºC and 35 % RH). The post-test characterization with fluorescent dye penetrant found small cracks only on the edges of the four-point specimen (Figure 24). It is likely that these small cracks were formed during the fabrication of this specimen.

Figure 23. Sandia Four-point bend test.

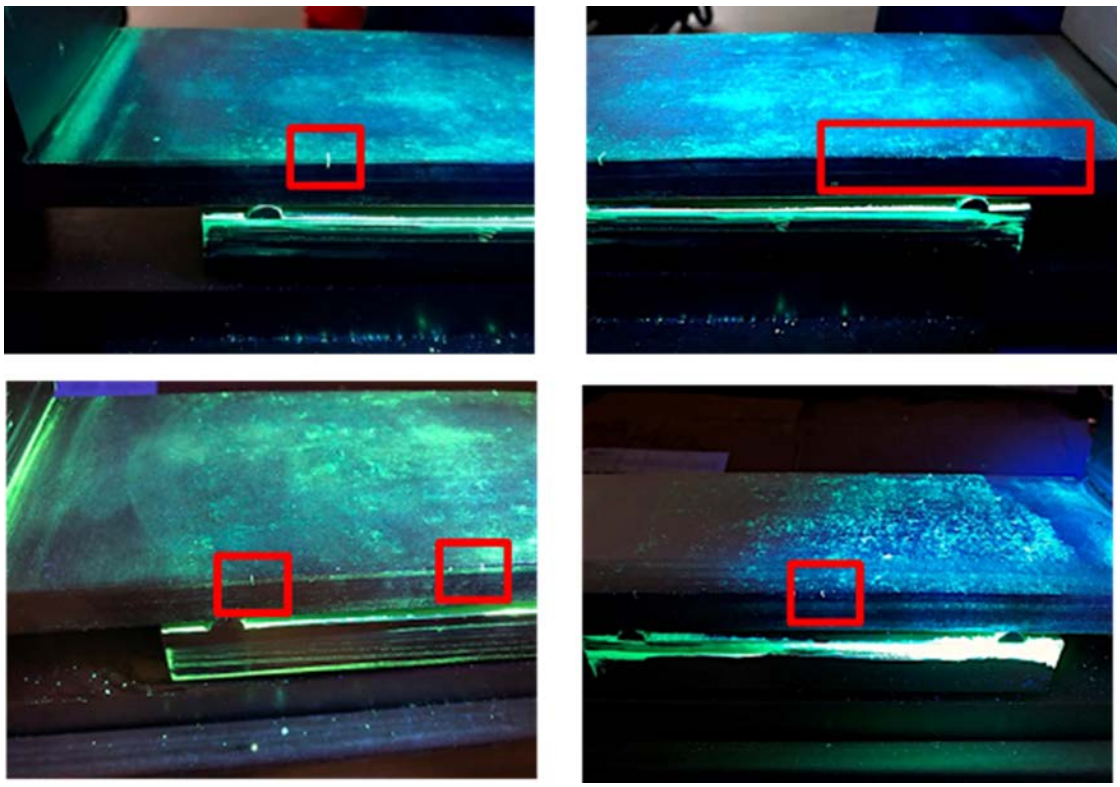

Figure 24. Dye penetrant analysis revealed small cracks on the edges of the 4-point bend specimen after testing at 80ºC and 35 % RH.

The Sandia big plate tests also included corrosion product and brine evolution analyses. It was found that the iron-containing corrosion products were largely amorphous and akageneite was identified by X-ray diffraction (XRD). The post-test brine analysis indicated that two distinct magnesium containing phases co-existed on the plate surface: (1) an Oxygen-rich/Chlorine-depleted compound, which is likely magnesium-hydroxychloride, $xMgO \cdot yMgCl_2 \cdot zH_2O$ (2-1-4 phase) and (2) a Chlorine-rich compound, which is likely bischofite, $MgCl_2 \cdot 6H_2O$.

4. ASME SECTION XI CODE CASE N-860 DEGRADATION ASSESSMENT

The ASME Section XI Code Case N-860 [2] is intended to provide inservice inspection requirements for examination of the accessible exterior metallic portions of the welded austenitic stainless steel SNF storage and transportation canisters. In Code Case N-860 Paragraph 2320 "Classification of Degradation," the visual anomaly shall be classified by degradation condition and location. The Japanese Industrial Standard, JIS G 0595, "Rating Method of Rust and Stain of Atmospheric Corrosion for Stainless Steels," [25] is used as an example to distinguish the severity between "major," "minor," or "insignificant" degradation. The JIS G 0595 uses Rating Numbers (RN) to quantify the rust coverage on a 100×150 mm sample, with RN 0 representing 100% coverage and RN 9 being 0.0093%. The Code Case N-860 recommended that RN 0 to 4 indicates "major" surface corrosion (rust coverage > 22% on a 100×150 mm sample); RN 5 to 6 indicates "minor" surface corrosion (3% < rust coverage < 15%); and RN 7 and greater indicates "insignificant" surface corrosion (rust coverage < 0.4%).

This section describes degradation assessment to characterize SRNL large plate using JIS G 0595 method as suggested in ASME Section XI Code Case N-860. The weld area of the SRNL large plate is shown in Figure 25, which was taken on October 16, 2019. It was found that no significant changes of corrosion appearance since then, even after extra salt load was applied to two of the starter cracks (Fig. 12). As shown in Figure 25, a strict application of JIS G 0595 with a sampling size of 100×150 mm is not practical. Therefore, the rust coverage was performed over a 30×50 mm area (about 1/3 of the linear dimensions as required by JIS N 0595) around the seed crack VP2. Note that the design crack length of VP2 on the plate surface is 12 mm.

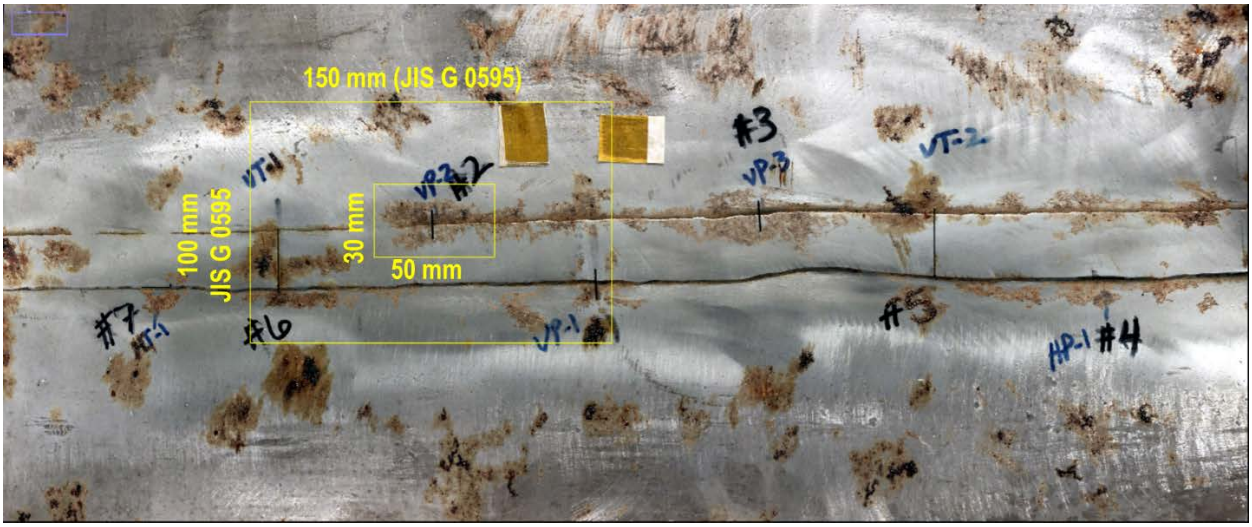

Figure 25. Rust coverage assessment for SRNL large plate: The yellow boxes represent JIS G 0595 region (100X150 mm), and a modified region (30X50 mm) currently used to evaluate starter crack VP2 and its vicinity, respectively.

The estimation for the rust coverage can be described in three steps: (1) Image processing was performed over the 30×50 mm sampling region around starter crack (Figure 26a); (2) Masking the un-corroded area in red over the sampling region (Figure 26b); and (3) Calculating the total pixel counts in the white area where the rust is identified (Figure 26c).

(a) (b) (c)

Figure 26. Image analysis to evaluate the rust coverage: sampled region (a), masking un-corroded area in red (b), and calculation of the white pixel counts in the rusted areas (c).

The pixel analysis result indicates that the corroded area in Figure 26c contains 170,403 pixels. With 420,336 total pixels in the entire sampling region (Figure 26a), the rust area ratio is 170,403/420,336= 40.5%. By JIS G 0595 designation, it is between RN 2 (47%) and RN 3 (32%).

By observing the Sandia big plate test images in Figures 21b and 22b, the corrosion condition appears more severe than the sampling region shown in Figure 26a. This is expected because Sandia big plates were heavily loaded with 8 g/m^2 of $MgCl_2$ and tested at 80 °C and 35% RH, and yet the SRNL large plate was loaded with less aggressive artificial sea salt with 2.3 grams Cl^-/m^2 and exposed to room temperature about 22 °C and 73% RH. If the same image process methodology would have been applied, the Sandia big plates would exceed RN 1 (69% rust coverage). Therefore, based on ASME Code Case N-860 recommendation, both Sandia and SRNL plates would be under the category of "major" surface corrosion (i.e., rust coverage > 22% on a 100×150 mm sample), and may require additional actions. On the other hand, if any corrosion is found in the weld region (Class C, as defined in Code Case N-860), then supplement examination such as surface or volumetric examination must be carried out, regardless of the surface corrosion classification (i.e., major, minor, or insignificant degradation). In the present case, both Sandia big plates and the SRNL large plate did not reveal any surface cracking for more than 15 months of exposure. It can be concluded that JIS G 0595 analysis is not sufficient to correlate CISCC to the surface corrosion condition.

5. PATH FORWARD

The SRNL large plate test was initiated in May 2019. The plate contains 7 starter cracks and was loaded with 2.3 grams/m^2 (Cl^-) of artificial sea salt on the outside surface (convex side) and exposed to room temperature (~22 °C) with constant RH of 73% in an enclosed test cell. In October 2019, two of the starter cracks were selected to add additional salt. Periodic inspection has been conducted but no CISCC was detected to date (15 months under exposure). It has been determined that the large plate be taken out of the test cell by May 2021 when two full years of exposure is complete. The plate will be first inspected by NDE to identify any existence of SCC on and inside the large plate. Then the materials surrounding some selected starter cracks will be separate from the plate for destructive examination by sectioning the samples into thin slices for metallurgical examination to reveal potential subsurface SCC and crack morphology.

5.1. Nondestructive Examination

Current NDE methods for SCC detection includes dye penetrant, eddy current, acoustic emission and electrochemical impedance spectroscopy (EIS) methods. Some of those techniques will be applied to the large plate after the test is complete and the plate is cleaned. In addition, new ultrasonic NDE methods that are being developed at the University of South Carolina under the DOE Nuclear Energy University Programs (NEUPs): (i) Ultrasonic guided wave (GW) method [26] and (ii) fully noncontact using pulsed laser (PL) method [27]. The SRNL large plate will also be characterized using these new NDE tools.

Figure 27 shows the concept of the GW method using a hybrid (contact and noncontact GW devices) piezoelectric transducer (PZT) – scanning laser Doppler vibrometer (SLDV) system. The actuation is implemented by a PZT bonded on the specimen surface using adhesives like M-

bond 200, and the wave sensing is achieved by SLDV, which is placed remotely and sends class II laser beam normal to the specimen. A large welded plate made of A285 carbon steel, previously tested in a Savannah River high level nuclear waste tank program [12], was used for demonstrating the PZT-SLDV capability. The stress corrosion cracks emanating from starter cracks were observed in about two weeks after this A285 large plate was immersed in 5 molar (5M) sodium nitrate ($NaNO_3$) solution at 90 ºC. The preliminary PZT-SLDV test showed that the SCC could be detected and the crack length was comparable with the magnetic particle test (MT) result, which was marked on the scanning region (red dotted box) as shown in Figure 27.

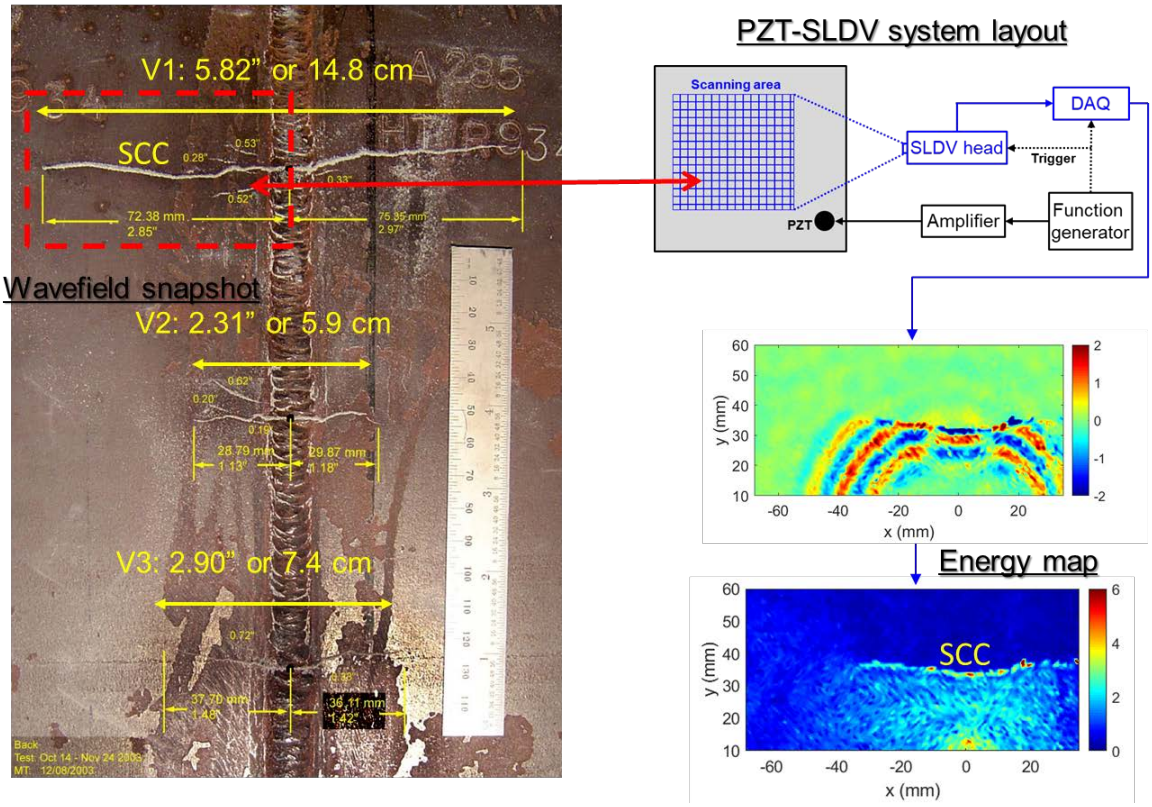

Figure 27. Schematic of a piezoelectric transducer – scanning laser Doppler vibrometer system (PZT-SLDV) to detect stress corrosion cracking

This A285 large plate with stress corrosion cracks (shown on the left-hand-side in Figure 27) was also used to develop a fully noncontact PL-SLDV method. In this case, a pulsed Q-switched laser is used for actuation instead of the PZT transducer. The class IV laser illuminates the surface of the plate, heats up locally, and excites the ultrasonic waves through thermoelastic effect. The wave sensing is also carried out by SLDV. The schematic of PL-SLDV inspection is shown in Figure 28, along with a preliminary result. For thick plate testing, the PL and SLDV need to be placed on the same side of the plate.

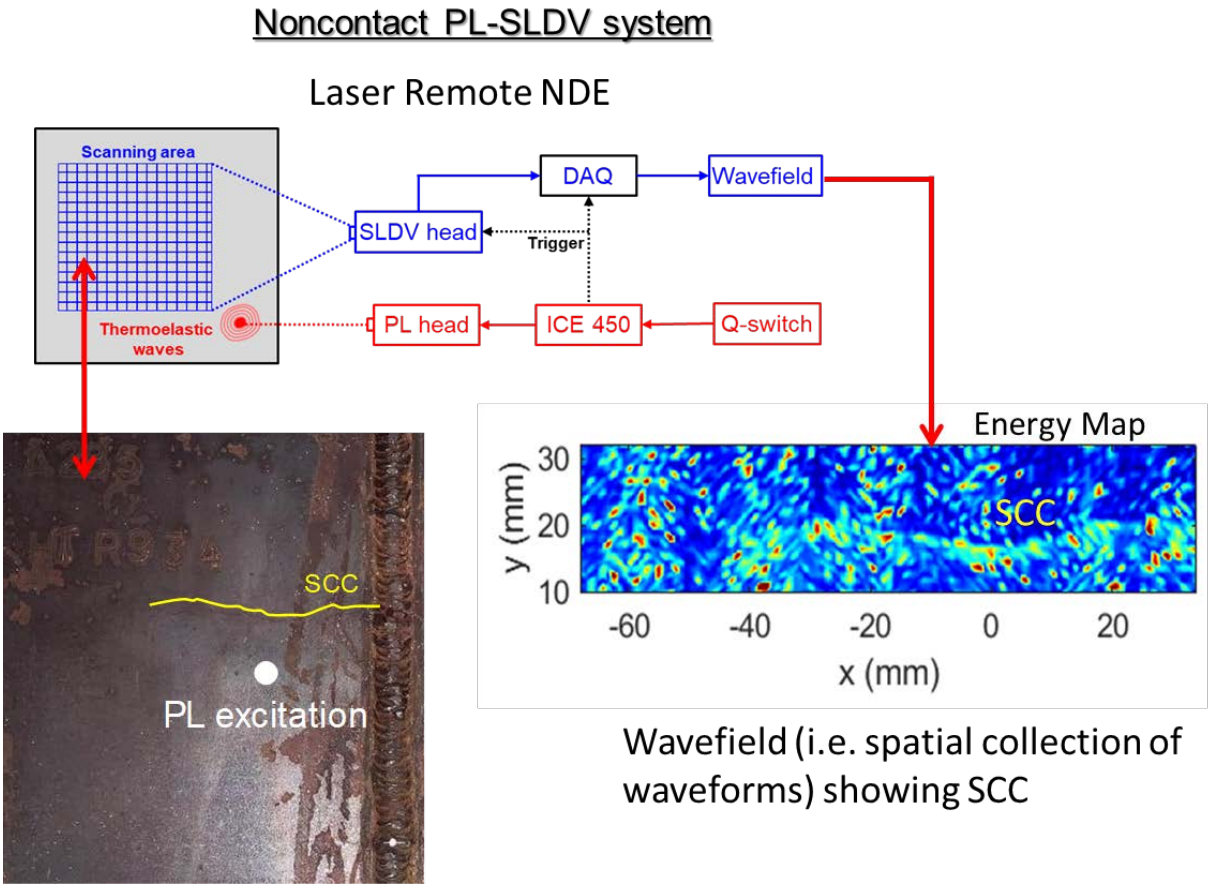

Figure 28. Schematic of a non-contact pulsed laser - scanning laser Doppler vibrometer System (PL-SLDV) to detect stress corrosion cracking

5.2. Destructive Examination

After the large plate is removed from the test cell following a two-year exposure duration on May 2021, it will be cleaned and inspected with various NDE techniques including visual inspection (VT), liquid dye penetrant testing (PT), and ultrasonic testing (UT). The presence of stress corrosion cracking will be carefully examined. Once NDE is complete, representative samples of starter cracks will be harvested out of the plate using EDM, followed by serial sectioning into thin slices at regular intervals along the depth of the flaw. The planned schematic is shown in Figure 29.

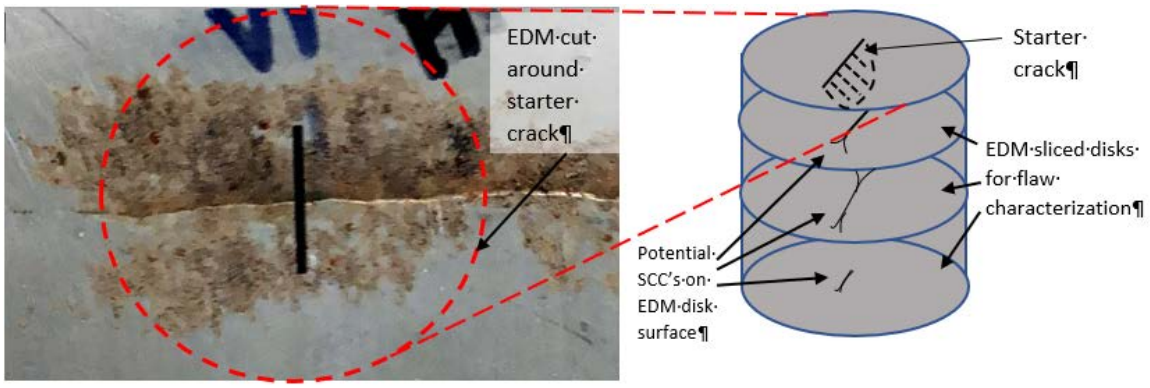

Figure 29. Schematic of serial sectioning of materials containing a starter crack along the depth of the stress corrosion crack.

6. CONCLUDING REMARKS

This report describes the large plate experiments as part of the stress corrosion cracking research for the long term performance of the spent nuclear fuel storage and transportation canisters in chloride-rich environments. Because post-weld heat treatment is not required for the fabrication of these canisters, the welding residual stress is considered as the main driving force for stress corrosion cracking.

Large plates, many containing fabrication welds, were harvested from a full size markup canister at Sandia National Laboratories [6] and distributed to various laboratories for stress corrosion tests. The large plate tested at Savannah River National Laboratory is a 51×46 cm section with a circumferential weld. Starter cracks were fabricated by EDM in the weld region of the plate. It is used to demonstrate stress corrosion cracking under naturally deliquescing condition of a thin layer of dry artificial sea salt on the large plate surface in 73% relative humidity at room temperature (typically 22 °C). The test was initiated in May 8, 2019 and periodic examination of the plate has been conducted. Based on API stress intensity factor calculations (Section 2.5) and the test data from the literature as shown in Figures 18 and 19, the starter cracks are expected to grow, provided that the as-fabricated welding residual stress was not significantly altered or redistributed by plate sectioning from the mockup canister and by EDM of the starter cracks. However, the incubation time of the stress corrosion cracking is unknown, but based on the Japanese natural exposure test data [17,18], it appears that the crack initiation might take about one to two years to occur under the Miyakojima climate (average 27 °C and 80% RH), which is similar to the Savannah River National Laboratory large plate test condition (room temperature about 22 °C and 73% RH). The SRNL large plate test is currently in progress. No stress corrosion cracks have been found on the plate surface so far, even active corrosion has been observed in the close vicinities of some starter cracks. This test will continue until May 2021, at which time two full years of exposure is complete. The plate will be taken out of the test cell and cleaned. NDE will be performed first and then followed by destructive examination by

slicing the material samples around the selected starter cracks to carefully inspect for stress corrosion cracks, and to validate the crack growth rate test results [5] and the crack growth rate model adopted by ASME Section XI Code Case N-860 [2,3] if CISCC is found.

Sandia National Laboratories also tested several "big plates," which were harvested from the same mockup canister. Those plates also contain fabrication welds but no starter cracks were machined. More aggressive salt, $MgCl_2$, was applied on the surfaces of the Sandia plates and the exposure condition was at 80 °C with 35% RH for 12 months. Significant corrosion products were found on the plate surfaces but the stress corrosion cracks were not found. Detailed chemical analyses were conducted for the corrosion products and the depleted brine on the plates. The Sandia tests provide critical information that supplements the findings from the Savannah River large plate test.

7. REFERENCES

[1] NRC Regulations, Title 10, Code of Federal Regulations, Part 72 (10 CFR 72) - Licensing Requirements for The Independent Storage of Spent Nuclear Fuel, High-Level Radioactive Waste, and Reactor-Related Greater Than Class C Waste, Subpart 72.42 "Duration of license; renewal," U. S. Nuclear Regulatory Commission, Washington DC, UAS.

[2] ASME Boiler and Pressure Vessel Section XI Code Case N-860: "Inspection Requirements and Evaluation Standards for Spent Nuclear Fuel Storage and Transportation Containment Systems," Board approved July 2020, in preparation for publication, American Society of Mechanical Engineers, New York, NY, USA.

[3] Broussard, J., Bryan, C., Sindelar, R., and Lam, P. S., 2019, "Crack Growth Rate Model for CISCC of Stainless Steel Canisters," Paper No. PVP2019-94055, Proceedings of ASME Pressure Vessels and Piping Conference, San Antonio, Texas, USA.

[4] Lam, P. S. and Kim, Y. J., 2016, I-NERI Project Number 2016-001-K: *Flaw Stability and Stress Corrosion Cracking of Austenitic Stainless Steel Canisters for Long Term Storage and Transportation of LWR Used Fuel*, U. S. Department of Energy - Office of Nuclear Energy, Washington D. C., USA.

[5] Lam, P. S., Duncan, A. J., and Sindelar, R. L., Crack Growth Rate and Large Plate Demonstration of Chloride-induced Stress Corrosion Cracking in Spent Nuclear Fuel Storage Canisters, Milestone No. M3SF-19SR010201052 (SRNL-STI-2019-00561), September 2019, Savannah River National Laboratory, Aiken, South Carolina, USA.

[6] Enos, D. G. and Bryan, C. R., 2016, *Final report: Characterization of Canister Mockup Weld Residual Stresses*, FCRD-UFD-2016-000064 Sandia National Laboratories, Albuquerque, New Mexico, USA.

[7] API 579-1/ASME FFS-1, 2007, Fitness-For-Service (API 579 Second Edition), American Petroleum Institute, Washington, DC., USA.

[8] API 579-1/ASME FFS-1, 2016, Fitness-For-Service, American Petroleum Institute, Washington, DC., USA.

[9] Lee, H. J., Kim, Y. J., Lam, P. S., and Sindelar, R. L., 2019, "Engineering J estimates for Spent Fuel Canisters under Combined Mechanical and Welding Residual Stresses," Paper Number PVP2019-93936, Proceedings of the ASME Pressure Vessels & Piping Conference, San Antonio, Texas, USA, July 2019.

[10] Lam, P. S., Duncan, A. J., Ward, L. N., Sindelar, R. L., Kim, Y. J., Jeong, J. Y., Lee, H. J., and Lee, M. W., 2019, "Crack Growth Rate Testing and Large Plate Demonstration under Chloride-Induced Stress Corrosion Cracking Conditions in Stainless Steel Canisters for Storage of Spent Nuclear Fuel," Paper Number PVP2019-94031, Proceedings of the ASME Pressure Vessels & Piping Conference, San Antonio, Texas, USA.

[11] Duncan, A. J., Lam, P. S. and Sindelar, R. L., 2020, "CISCC Experiment of a Large Plate Sectioned from a Spent Nuclear Fuel Canister," Paper No. PVP2020-21774, Proceedings of the ASME Pressure Vessels & Piping Conference, Minneapolis, Minnesota, USA, July 2020.

[12] Lam, P. S., Chang, C., Chao, Y. J., Sindelar, R. L., Stefek, T. M., and Elder III, J. B., 2005, “Stress Corrosion Cracking of Carbon Steel Weldments,” Paper Number PVP2005-71327, Proceedings of ASME Pressure Vessels and Piping Conference, Denver, Colorado, USA.

[13] Lam, P. S., 2009, Investigation of the Potential for Caustic Stress Corrosion Cracking of A537 Carbon Steel Nuclear Waste Tanks, SRNS-STI-2009-00564 Rev.1, Savannah River Nuclear Solutions, Aiken, South Carolina, USA.

[14] Lam, P. S., Stripling, C. S., Fisher, D. L., and Elder III, J. B., 2010, “Potential for Stress Corrosion Cracking of A537 Carbon Steel Nuclear Waste Tanks Containing Highly Caustic Solutions,” Paper No. PVP2010-25117, Proceedings of ASME Pressure Vessels and Piping Conference, Bellevue, Washington, USA.

[15] Gim, J. M., Kim, J. S., Kim, Y. J., and Lam, P. S., 2018, “FE welding residual stress analysis and validation for spent nuclear fuel canisters,” Paper Number PVP2018-84857, Proceedings ASME Pressure Vessels & Piping Conference, Prague, Czech Republic.

[16] Wang, J. A., Payzant, A., Bunn, J., and An, K., 2018, *Neutron Residual Stress mapping for Spent Nuclear Fuel Storage Canister Weldment*, ORNL/TM-2018/827, Oak Ridge, Tennessee, USA.

[17] Kosaki, A., 2006, “SCC Propagation Rate of Type 304, 304L Steels under Oceanic Air Environment,” Paper No. ICONE14-89271, Vol. 1, Plant Operations, Maintenance and Life Cycle; Component Reliability and Materials Issues; Codes, Standards, Licensing and

Regulatory Issues; Fuel Cycle and High Level Waste Management, International Conference on Nuclear Engineering, July 17-20, Miami, Florida, USA, pp. 443-450.

[18] Kosaki, A., 2008, "Evaluation Method of Corrosion Lifetime of Conventional Stainless Steel Canister under Oceanic Air Environment," Nuclear Engineering and Design, 238, pp. 1233-1240.

[19] Relative Humidity in Miyakojima, Japan, http://www.miyakojima.climatemps.com/humidity.php

[21] Jeong, J. Y., Lee, M. W., Kim, Y. J., Sindelar, R., and Duncan, A., 2019, "Development of an apparatus for chloride induced stress corrosion cracking test using immersion method with constant displacement condition," Paper No. PVP2019-93922, Proceedings of ASME Pressure Vessels and Piping Conference, San Antonio, Texas, USA.

[22] Jeong, J. Y., Lee, M. W., Kim, Y. J., Lam, P. S., and Duncan, A. J., 2020, "Chloride-Induced Stress Corrosion Cracking Tester for Austenitic Stainless Steel," Journal of Testing and Evaluation, 49, Published ahead of print, 03 August 2020, ASTM International, West Conshohocken, Pennsylvania, USA. (https://doi.org/10.1520/JTE20200115)

[23] Tani, J., Mayuzumi, M., Arai, T., and Hara, N., 2007, "Stress Corrosion Cracking Growth Rates of Candidate Canister Materials for Spent Nuclear Fuel Storage in Chloride-Containing Atmosphere," Materials Transactions, Vol. 48, No. 6, pp. 1431 to 1437.

[24] Bryan, C. R., Schaller, R. F., Knight, A. W., and Schindelholz, E. J., Electric Power Research Institute (EPRI) Extended Storage Collaboration Program (ESCP) Fall Meeting, Charlotte, SC November 6, 2019, https://www.osti.gov/servlets/purl/1646222.

[25] Japanese Industrial Standard, "Rating Method of Rust and Stain of Atmospheric Corrosion for Stainless Steels," JIS G 0595: 2004, Translated to English by Japanese Standards Association, January 2005.

[26] Yu, L., DOE Nuclear Energy University Program 2020, "Engineered composite patch with NDE inspection for repair and mitigation of SCC in nuclear spent fuel dry storage canister," University of South Carolina, Columbia, SC., USA.

[27] Yu, L., DOE Nuclear Energy University Program 2019, "Remote laser based nondestructive evaluation for post irradiation examination of accident tolerant fuel (ATF) cladding," University of South Carolina, Columbia, SC., USA.